Axonal distribution of mitochondria maintains neuronal autophagy during aging via eIF2β

Kanako Shinno[1†], Yuri Miura[2], Koichi M. Iijima[3,4], Emiko Suzuki[1,5], Kanae Ando[1,6*]

1. Department of Biological Sciences, Graduate School of Science, Tokyo Metropolitan University, Hachioji, Tokyo, 192-0397, Japan
2. Research Team for Mechanism of Aging, Tokyo Metropolitan Institute for Geriatrics and Gerontology, Itabashi, Tokyo, 173-0015, Japan
3. Department of Alzheimer's Disease Research, National Center for Geriatrics and Gerontology, Obu, Aichi, 474-8511, Japan
4. Department of Experimental Gerontology, Graduate School of Pharmaceutical Sciences, Nagoya City University, Nagoya, Aichi, 467-8603, Japan
5. Gene Network Laboratory, National Institute of Genetics and Department of Genetics, SOKENDAI, Mishima, Shizuoka, 411-8540, Japan
6. Department of Biological Sciences, School of Science, Tokyo Metropolitan University, Hachioji, Tokyo, 192-0397, Japan

*Correspondence: k_ando@tmu.ac.jp

[†]Current address: Department of Neuroscience and Pathobiology, Research Institute of Environmental Medicine, Nagoya University, Chikusa-Ku, Nagoya, Aichi, 464-8601, Japan

Summary

Neuronal aging and neurodegenerative diseases are accompanied by proteostasis collapse, while the cellular factors that trigger it have not been identified. Impaired mitochondrial transport in the axon is another feature of aging and neurodegenerative diseases. Using *Drosophila*, we found that genetic depletion of axonal mitochondria causes dysregulation of protein degradation. Axons with mitochondrial depletion showed abnormal protein accumulation and autophagic defects. Lowering neuronal ATP levels by blocking glycolysis did not reduce autophagy, suggesting that autophagic defects are associated with mitochondrial distribution. We found that eIF2β was increased by the depletion of axonal mitochondria via proteome analysis.

Phosphorylation of eIF2α, another subunit of eIF2, was lowered, and global translation was suppressed. Neuronal overexpression of *eIF2β* phenocopied the autophagic defects and neuronal dysfunctions, and lowering *eIF2β* expression rescued those perturbations caused by depletion of axonal mitochondria. These results indicate the mitochondria-eIF2β axis maintains proteostasis in the axon, of which disruption may underlie the onset and progression of age-related neurodegenerative diseases.

Highlights

- Loss of axonal mitochondria impairs autophagy and accumulates proteins in the axon
- Loss of axonal mitochondria increases eIF2β and decreases p-eIF2α
- Neuronal upregulation of eIF2β induces autophagic defects and locomotor dysfunction
- Lowering eIF2β rescues autophagic defects caused by loss of axonal mitochondria

Keywords

Mitochondria; axonal transport; aging; neuronal proteostasis; protein aggregation; autophagy; eukaryotic Initiation Factor 2β (eIF2β); *Drosophila*; neurodegeneration; proteome

Introduction

Neurons have a morphologically complex architecture composed of microcompartments and require tight regulation of the abundance of proteins and organelles spatially and temporally[1]. Such control of protein amounts, or proteostasis, is essential for neuronal functions[2] and is achieved through the orchestration of protein expression, folding, trafficking, and degradation controlled by intrinsic and environmental signals[3]. Translation is initiated by the eukaryotic initiation factor 2 (eIF2) complex[4]. eIF2, a heterotrimer of α, β, and γ subunits, transports Met-tRNA to the ribosome in a GTP-dependent manner[5]. Under stressed conditions, phosphorylation of eIF2α attenuates global translation and initiates translation of mRNAs related to the integrated stress response (ISR)[6]. As for protein degradation, autophagy and proteasome are major systems that maintain proteostasis[7]. The proteasome degrades unnecessary proteins,

71 followed by regulated ubiquitination processes[8], and autophagy removes damaged or
72 harmful components, including large protein aggregates and organelles, through
73 catabolism (selective autophagy)[9]. In addition to autophagy induced by acute stressors,
74 a basal level of selective autophagy mediates the global turnover of damaged proteins[10].
75
76 Such constitutive autophagy decreases during aging, which may underlie declines in the
77 structural and functional integrity of neurons[11]. Decreased protein degradation and
78 accumulation of abnormal proteins also contribute to increased risks of
79 neurodegenerative diseases. Age-related neurodegenerative diseases such as
80 Alzheimer's disease and Parkinson's disease are often associated with the accumulation
81 of misfolded proteins such as amyloid-β, tau, and α-synuclein[12]. Enhancement of
82 autophagy mitigates age-related dysfunctions and neurodegeneration caused by
83 proteotoxic stress[13]. However, it is not fully understood how aging disrupts the
84 regulation of this constitutive autophagy.
85
86 Neurons are also highly energy-demanding cells. At nerve terminals, action potentials
87 trigger the release of neurotransmitters via exocytosis of synaptic vesicles, which
88 requires a constant supply of ATP and calcium buffering[14]. Such neuronal activity relies
89 on mitochondrial functions[15], and mitochondria are actively transported from their
90 major sites of biogenesis in soma to axons[16]. However, the axonal transport of
91 mitochondria declines during aging[17,18,19]. Reduced axonal transport of mitochondria is
92 thought to contribute to age-related declines in neuronal functions[17,19,20,21]. The number
93 of functional mitochondria in synapses is reduced in the brains of patients suffering
94 from age-related neurodegenerative diseases such as Alzheimer's disease[22], and
95 mutations in genes involved in mitochondrial dynamics are linked to neurodegenerative
96 diseases[23]. The mislocalization of mitochondria is sufficient to cause age-dependent
97 neurodegeneration in *Drosophila* and mice[24,25], indicating that the proper distribution of
98 mitochondria is essential to maintain neuronal functions. Thus, depletion of functional
99 mitochondria from axons and proteostasis collapse are common features of aging and
100 neurodegenerative diseases.
101
102 Mitochondrial transport is regulated by a series of molecular adaptors that mediate the
103 attachment of mitochondria to molecular motors[16]. In *Drosophila*, mitochondrial
104 transport is mediated by milton and Miro, which attaches mitochondria to microtubules
105 via kinesin heavy chain[26,27]. In the absence of milton or Miro, synaptic terminals and
106 axons lack mitochondria, although mitochondria are numerous in the neuronal cell

body[28]. We previously reported that RNAi-mediated knockdown of *milton* or *Miro* in neurons causes a reduction in axonal mitochondria, age-dependent locomotor defects[29], and age-dependent neurodegeneration in neuropile area starting around 30 days after eclosion (day-old)[24], and enhances axon degeneration caused by human tau proteins[24], suggesting that these flies can be used as a model to analyze the effect of depletion of axonal mitochondria during aging. In this study, we investigated a causal relationship between mitochondrial distribution and neuronal proteostasis by using neuronal knockdown of *milton*. We found that depletion of axonal mitochondria reduced autophagy and increased the accumulation of aggregated proteins in the axon prior to gross neurodegeneration. Proteome analysis and follow-up biochemical analyses revealed that neuronal knockdown of *milton* increased eIF2β levels and lowered phosphorylation of eIF2αin the axon. In addition, *milton* knockdown suppressed global translation. Overexpression of *eIF2β* was sufficient to decrease autophagy and induce neuronal dysfunction, and genetic suppression of *eIF2β* restored autophagy and improved neuronal function in the *milton* knockdown background. These findings suggest that loss of axonal mitochondria and elevated levels of eIF2β mediate proteostasis collapse and neuronal dysfunction during aging.

Results

Depletion of axonal mitochondria by knockdown of *milton* or *Miro* causes protein accumulation in the axon

In *Drosophila*, mitochondrial transport is mediated by milton and Miro, which attach mitochondria to microtubules via kinesin heavy chain[26,27] (Figure 1A). It has been reported that expression of *milton* RNAi in neurons via pan-neuronal elav-GAL4 driver reduced milton protein levels in *Drosophila* head lysate to 40% and mito-GFP signals in axons to 50%[24,29].

To test how loss of axonal mitochondria affects proteostasis in neurons, we first examined the accumulation of ubiquitinated proteins. At 14-day-old, more ubiquitinated proteins were deposited in the brains of *milton* knockdown flies than in those of age-matched control flies (Figure 1B, $p < 0.005$ between control RNAi and *milton* RNAi). There was no significant increase in ubiquitinated proteins in *milton* knockdown flies at 1-day old, suggesting that the accumulation of ubiquitinated proteins caused by *milton* knockdown is age-dependent (Figure S1). We also analyzed the effect of the neuronal knockdown of *Miro*, a partner of milton, on the accumulation of

143 ubiquitin-positive proteins. Since severe knockdown of *Miro* in neurons causes lethality,
144 we used UAS-*Miro* RNAi strain with low knockdown efficiency, whose expression
145 driven by elav-GAL4 caused 30% reduction of *Miro* mRNA in head extract[24]. Although
146 there was a tendency for increased ubiquitin-positive puncta in *Miro* knockdown brains,
147 the difference was not significant (Figure 1B, $p>0.05$ between control RNAi and *Miro*
148 RNAi). These data suggest that the depletion of axonal mitochondria induced by *milton*
149 knockdown leads to the accumulation of ubiquitinated proteins before
150 neurodegeneration occurs.
151 It has been reported that ubiquitinated proteins accumulate with aging[30]; thus, we
152 analyzed the accumulation of ubiquitinated proteins in aged brains (30-day-old) with
153 *milton* knockdown. The number of puncta of ubiquitinated proteins did not significantly
154 differ between control and *milton* knockdown flies or between control and *Miro*
155 knockdown flies (Figure 1C, $p > 0.05$). These results suggest that depletion of axonal
156 mitochondria may have more impact on proteostasis in young neurons than in old
157 neurons.
158 We examined the ultrastructure of presynaptic terminals and cell bodies in
159 photoreceptor neurons with *milton* knockdown by transmission electron microscopy in
160 27-day-old flies (Figure 1D). As previously reported[24], the number of mitochondria in
161 presynaptic terminals decreased in *milton* knockdown (Figure 1E). The swelling of
162 presynaptic terminals, characterized by the enlargement and roundness, was not
163 reported at 3-day-old[24] but observed at this age with about 4% of total presynaptic
164 terminals (Figure 1F, asterisks).
165 Some presynaptic terminals of *milton* knockdown neurons contained dense materials
166 (Figure 1F and G, arrowheads). Dense materials are rarely found in age-matched control
167 neurons, indicating that *milton* knockdown induces abnormal protein accumulation in
168 the presynaptic terminals (Figure 1G and H). In *milton* knockdown neurons, dense
169 materials are found in swollen presynaptic terminals more often than in presynaptic
170 terminals without swelling, suggesting a positive correlation between the disruption of
171 proteostasis and axonal damage (Figure 1G). In contrast, dense materials were not
172 observed in cell bodies in the *milton* knockdown retina (Figure 1H). These results
173 indicate that the depletion of axonal mitochondria induces protein accumulation in the
174 axon.
175
176 **Depletion of axonal mitochondria impairs protein degradation pathways**
177 Since abnormal proteins were accumulated in *milton* knockdown brains, we next
178 examined if protein degradation pathways were suppressed. We analyzed autophagy via

179 western blotting of the autophagy markers LC3 and p62[31]. During autophagy
180 progression, LC3 is conjugated with phosphatidylethanolamine to form LC3-II, which
181 localizes to isolation membranes and autophagosomes. LC3-I accumulation occurs
182 when autophagosome formation is impaired, and LC3-II accumulation is associated
183 with lysosomal defects[31,32]. p62 is an autophagy substrate, and its accumulation suggests
184 autophagic defects[31,32]. We found that *milton* knockdown increased LC3-I, and the
185 LC3-II/LC3-I ratio was lower in *milton* knockdown flies than in control flies at
186 14-day-old (Figure 2A). We also analyzed p62 levels in head lysates sequentially
187 extracted using detergents with different stringencies (1% Triton X-100 and 2% SDS).
188 Western blotting revealed that p62 levels were increased in the brains of 14-day-old of
189 *milton* knockdown flies (Figure 2B). The increase in the p62 level was significant in the
190 Triton X-100-soluble fraction but not in the SDS-soluble fraction (Figure 2B),
191 suggesting that depletion of axonal mitochondria impairs the degradation of
192 less-aggregated proteins. Proteasome activity was also significantly decreased in brains
193 with neuronal knockdown of *milton* (Figure 2C, $p < 0.005$).
194 At 30-day-old, LC3-I was still higher, and the LC3-II/LC3-I ratio was lower, in *milton*
195 knockdown compared to the control (Figure 2D). At this age, *milton* knockdown
196 increased p62 significantly in 1% Triton X-100 fraction and 2% SDS fraction (Figure
197 2E). Proteasome activities were also decreased in *milton* knockdown flies at 30-day-old
198 (Figure 2F). These results indicate that depletion of axonal mitochondria impairs protein
199 degradation pathways.
200
201 **ATP deprivation does not impair autophagy**
202 *milton* knockdown downregulates ATP in the axon[33]. To examine whether the disruption
203 of protein degradation pathways by *milton* knockdown is due to ATP deprivation, we
204 investigated the effects of knocking down phosphofructokinase (*Pfk*), a rate-limiting
205 enzyme in glycolysis, on protein degradation pathways. Neuronal knockdown of *Pfk*
206 was reported to lower ATP levels in brain neurons[33]. *Pfk* knockdown and *milton*
207 knockdown decreased ATP to similar levels (Figure 3A-C). However, in contrast with
208 *milton* knockdown, *Pfk* knockdown did not affect the levels of LC3-I, LC3-II or the
209 LC3-II/LC3-I ratio (Figure 3D). *Pfk* knockdown decreased p62 level (Figure 3E),
210 suggesting that autophagy is promoted. On the other hand, proteasome activity was
211 decreased by *Pfk* knockdown (Figure 3F). These results suggest that the downregulation
212 of axonal ATP upon depletion of axonal mitochondria decreases proteasome activity, but
213 not autophagy.
214

Proteome analysis suggests that depletion of axonal mitochondria causes disruption of autophagy and premature aging

To identify the pathways that mediate the decrease in autophagy in *milton* knockdown brains, we performed proteome analysis to systematically detect differentially expressed proteins upon neuronal knockdown of *milton*. We analyzed flies at 7- and 21-day-old, the age before autophagic defects are detected and the age just before the onset of neurodegeneration, respectively (Figure 4A). 1039 proteins were detected by liquid chromatography-tandem mass spectrometry (LC-MS/MS). Expression of 36 proteins was significantly increased (22 proteins) or decreased (14 proteins) by *milton* knockdown at 7-day-old (Figure 4B, Tables 1 and S1). At 21-day-old, the expression of 41 proteins (31 upregulated and ten downregulated proteins) was significantly altered in *milton* knockdown flies compared with control flies (Figure 4C, Tables 1 and S1). The "Interaction search" algorithm using KeyMolnet showed that proteins whose expression was significantly altered in the brains of *milton* knockdown flies at both 7- and 21-day-old were closely associated with the autophagic pathway (Table 2). Proteins involved in pathways characteristics of aging, such as the immune response (Transcriptional regulation by STAT), cancer (Transcriptional regulation by SMAD, Transcriptional regulation by myc), longevity (Transcriptional regulation by FOXO, Sirtuin signaling pathway), and stress responses (HSP90 signaling pathway, MAPK signaling pathway)[34,35], were enriched in the proteome profiles of *milton* knockdown flies compared with those of control flies at 7-day-old (Table 2), suggesting that depletion of axonal mitochondria accelerates aging in the brain.

Depletion of axonal mitochondria upregulates eIF2β and decreases phosphorylation of eIF2α

Differentially expressed proteins at 7-day-old flies may reflect alterations that are causal for autophagic defects. We noticed that the expression level of eIF2β was 2.465-fold higher in the brains of *milton* knockdown flies than in those of control flies (Figure 4B and D). Upregulation of eIF2β in the brains of *milton* knockdown flies was confirmed by western blotting. *milton* knockdown increased eIF2β protein levels more than twice (Figure 4E), but did not change the level of *eIF2β* mRNA (Figure 4F).

We also investigated age-dependent changes in eIF2β by western blotting of control flies at 7-, 21-, 35-, and 49-, and 63-day-old. eIF2β levels increased during aging until 49-day-old (Figure 4G). These results suggest that upregulation of eIF2β in *milton* knockdown fly brain reflects early an onset of age-dependent increase of eIF2β levels.

eIF2β is a subunit of the eukaryotic initiation factor 2 (eIF2) complex, which is critical

251 for translation initiation and the integrated stress response (ISR)[4]. eIF2 is a heterotrimer
252 of α, β, and γ subunits, and eIF2α is phosphorylated during the ISR[6]. As for the other
253 subunits of eIF2 complex, proteome analysis did not detect a significant difference in
254 the protein levels of eIF2α and eIF2γ between *milton* knockdown and control flies at 7-
255 and 21-day-old (Figure 4D). Western blotting of brain lysates showed that *milton*
256 knockdown reduced eIF2α levels (Figure 5A), while p-eIF2α levels were not
257 significantly affected (Figure 5B).
258 To analyze local changes of eIF2α and p-eIF2α, we carried out immunostaining. We
259 focused on the mushroom body, where axons, dendrites, and cell bodies can be easily
260 identified (Figure 5C). Both eIF2α and p-eIF2α were downregulated in the cell body
261 (Kenyon cells) and dendritic (Calyxes) regions of the brains of *milton* knockdown flies
262 (Figure 5D). In axons (lobe tips), *milton* knockdown did not affect eIF2α (Figure 5E, p
263 = 0.271) but significantly downregulated p-eIF2α (Figure 5E). The ratio of p-eIF2α to
264 eIF2α was lower in the axon but not in the soma or dendritic region. These results
265 suggest that axonal distribution of mitochondria regulate the level of overall eIF2α
266 protein and local p-eIF2α.
267
268 **Depletion of axonal mitochondria suppressed global translation**
269 Phosphorylation of eIF2α induces conformational changes in the eIF2 complex and
270 inhibits global translation[36]. To analyze the effects of *milton* knockdown on translation,
271 we performed polysome gradient centrifugation to examine the level of ribosome
272 binding to mRNA. Since p-eIF2α was downregulated, we hypothesized that *milton*
273 knockdown would enhance translation. However, unexpectedly, we found that *milton*
274 knockdown significantly reduced the level of mRNAs associated with polysomes
275 (Figure 6A and B). We also compared the level of translation between the brains of
276 control and *milton* knockdown flies by assessing the incorporation of puromycin (Figure
277 6C). Puromycin incorporation was lower in the brains of *milton* knockdown flies than in
278 those of control flies, while it was not statistically significant (Figure 6C, indicated by a
279 bracket). These data suggest that the depletion of axonal mitochondria suppresses global
280 translation.
281
282 **eIF2β upregulation reduces the level of p-eIF2α, impairs autophagy, and decreases**
283 **locomotor function**
284 We were motivated to ask if eIF2β upregulation mediates autophagic defects caused by
285 *milton* knockdown. If so, neuronal overexpression of *eIF2β* would also induce
286 autophagy impairment. Neuronal overexpression of *eIF2β* increased LC3-II, while the

287 LC3-II/LC3-I ratio was not significantly different (Figure 7A and B). Overexpression of
288 *eIF2β* significantly increased the p62 level in the Triton X-100-soluble fraction (Figure
289 7C, 4-fold vs. control, $p < 0.005$ (1% Triton X-100)) but not in the SDS-soluble fraction
290 (Figure 7C, 2-fold vs. control, $p = 0.062$ (2% SDS)), as observed in brains of *milton*
291 knockdown flies (Figure 2B). These data suggest that neuronal overexpression of *eIF2β*
292 accumulates autophagic substrates.
293 Since *milton* knockdown reduced the p-eIF2α level (Figure 5E), we asked whether an
294 increase in eIF2β affects p-eIF2α. Neuronal overexpression of *eIF2β* did not affect the
295 eIF2α level but significantly decreased the p-eIF2α level (Figure 7D and E).
296 Depletion of axonal mitochondria causes age-dependent decline in locomotor function[24].
297 We found that neuronal overexpression of *eIF2β* also caused locomotor dysfunction
298 (Figure 7F). Locomotor functions were significantly impaired in those flies at
299 20-day-old and worsened further during aging (Figure 7F, compare 4-, 20-, and
300 30-day-old). We asked if *eIF2β* overexpression causes neurodegeneration, as depletion
301 of axonal mitochondria in the photoreceptor neurons causes axon degeneration in an
302 age-dependent manner[24]. *eIF2β* overexpression in photoreceptor neurons tends to
303 increase neurodegeneration in aged flies, while it was not statistically significant
304 ($p>0.05$, Figure S2).
305 These data indicate that an increase of eIF2β in neurons phenocopies depletion of
306 axonal mitochondria, including suppression of autophagy and age-dependent locomotor
307 dysfunction, and suggest that increase of eIF2β mediates these phenotypes downstream
308 of loss of axonal mitochondria.
309
310 **Lowering *eIF2β* rescues autophagic impairment and locomotor dysfunction**
311 **induced by *milton* knockdown**
312 Finally, we investigated whether suppression of eIF2β rescues autophagy impairment
313 and locomotor dysfunction caused by neuronal knockdown of *milton*. Null mutants and
314 flies with RNAi-mediated knockdown of *eIF2β* in neurons did not survive. Flies lacking
315 one copy of the *eIF2β* gene survived without any gross abnormality, and the level of
316 *eIF2β* mRNA in these flies was about 80% of that in control flies (Figure 8A). *eIF2β*
317 heterozygosity did not affect the eIF2α and p-eIF2α levels (Figure S3A and B).
318 Neuronal knockdown of *milton* causes accumulation of autophagic substrate p62 in the
319 Triton X-100-soluble fraction (Figure 2B), and we tested if lowering eIF2β ameliorates
320 it. We found that *eIF2β* heterozygosity caused a mild increase in LC3-I levels and
321 decreases in LC3-II levels, resulting in a significantly lower LC3-II/LC3-I ratio in
322 *milton* knockdown flies (Figure 8B). *eIF2β* heterozygosity decreased the p62 level in

323 the Triton X-100-soluble fraction in the brains of *milton* knockdown flies (Figure 8C).
324 The p62 level in the SDS-soluble fraction, which is not sensitive to *milton* knockdown
325 (Figure 2B), was not affected (Figure 8C). These results suggest that suppression of
326 *eIF2β* ameliorates the impairment of autophagy caused by *milton* knockdown.
327 *eIF2β* heterozygosity also rescued locomotor dysfunction induced by *milton* knockdown.
328 *milton* knockdown flies with *eIF2β* heterozygosity exhibited better locomotor function
329 than *milton* knockdown alone (Figure 8D). The *milton* mRNA level was not increased in
330 these flies, indicating that the rescue effect in the *eIF2β* heterozygous background was
331 not mediated by an increase in the *milton* mRNA level (Figure S3C). These data suggest
332 that eIF2β upregulation mediates autophagy impairment and locomotor dysfunction
333 caused by the depletion of axonal mitochondria.
334
335
336 **Discussion**
337 The depletion of axonal mitochondria and accumulation of abnormal proteins are both
338 characteristics of aged brains[37,38]. Proteostasis perturbations trigger the formation of
339 pathological aggregates and increase the risks of neurodegenerative diseases during
340 aging. By using neuronal *milton* knockdown to deplete mitochondria from the axon, we
341 provide evidence that loss of axonal mitochondria drives age-related proteostasis
342 collapse via eIF2β (Figure 9). We observed declines in autophagy-mediated degradation
343 of less-aggregated proteins and proteasome activity in *milton* knockdown flies (Figure
344 2). Accumulation of ubiquitinated proteins and changes in age-related pathways started
345 prematurely in *milton* knockdown flies (Figure 1 and Table 2). *milton* knockdown
346 increased eIF2β and lowered eIF2α phosphorylation in young fly brain (Figure 4 and 5).
347 Overexpression of *eIF2β* phenocopied the effects of *milton* knockdown, including
348 reduced autophagy and accelerated age-related locomotor defects (Figure 7).
349 Furthermore, lowering *eIF2β* levels suppressed the impairment of autophagy and
350 locomotor dysfunction induced by *milton* knockdown (Figure 8). From these results, we
351 propose that upregulation of eIF2β downstream of depletion of axonal mitochondria
352 drives age-dependent collapse of proteostasis (Figure 9). Our results suggest that
353 mitochondrial distribution and eIF2β are part of the mechanisms constituting
354 proteostasis.
355
356 *milton* knockdown causes loss of mitochondria in the axon and accumulation of
357 mitochondria in the soma. Thus, the detrimental effects may be mediated by the
358 accumulation of mitochondria. However, degeneration induced by *milton* knockdown is

359 prominent in the axon and not detected in the cell body[24]. Furthermore, abnormal
360 protein accumulation was observed in the axon (Figure 1), and p-eIF2α/eIF2α was
361 decreased in the neurites but not in the soma (Figure 5), suggesting that proteostasis
362 defects studied in this work are caused by depletion of mitochondria rather than
363 accumulation of mitochondria. Further analyses to dissect the effects of *milton*
364 knockdown on proteostasis and translation in the cell body and axon by experiments
365 with spatial resolution would be needed.
366
367 Our results suggest that the loss of axonal mitochondria is an event upstream of
368 proteostasis collapse during aging. The number of puncta of ubiquitinated proteins was
369 higher in milton knockdown at 14-day-old, but there was no significant difference at
370 30-day-old (Figure 1). Proteome analyses also showed that age-related pathways, such
371 as immune responses, are enhanced in young flies with *milton* knockdown (Table 2). We
372 also found that eIF2β protein levels increase in an age-dependent manner until
373 49-day-old and reduces after that (Figure 4G). In the brains with neuronal knockdown
374 of *milton*, eIF2β levels were higher at 7-day-old than those in control and lower at the
375 21-day-old (Figure 4D and Supplementary table). These results suggest that *milton*
376 knockdown is likely accelerating age-dependent changes rather than increasing their
377 magnitude. Disruption of proteostasis is expected to contribute neurodegeneration[38] ,
378 and it would be interesting to analyze the sequence of protein accumulation and axonal
379 degeneration in *milton* knockdown ([24,29] and Figure 1) in detail with higher time
380 resolution.
381
382 Our results revealed that eIF2β regulates autophagy and maintains proteostasis during
383 aging. eIF2β is a component of eIF2, which meditates translational regulation and ISR
384 initiation. When ISR is activated, phosphorylated eIF2α suppresses global translation
385 and induces translation of ATF4, which mediates transcription of autophagy-related
386 genes[39,40]. Since ISR can positively regulate autophagy, we suspected that suppression
387 of ISR underlies a reduction in autophagic protein degradation. We found neuronal
388 knockdown of *milton* reduced phosphorylated eIF2α, suggesting that ISR is reduced
389 (Figure 5). However, we also found that global translation was reduced (Figure 6).
390 Increased levels of eIF2β might disrupt the eIF2 complex or alter its functions. The
391 stoichiometric mismatch caused by an imbalance of eIF2 components may inhibit ISR
392 induction. Supporting this model, we found that eIF2β upregulation reduced the levels
393 of p-eIF2α (Figure 7). It is also possible that eIF2β mediates autophagy defects via
394 mechanisms independent of ISR since eIF2β has functions independent of eIF2[41,42]. For

395 example, suppression of *eIF2β* has been reported to slow down cancer cell growth[41]. In
396 developing neurons, eIF2β can directly interact with the translational repressor Kra to
397 regulate midline axon guidance[42]. However, to our knowledge, the roles of eIF2β in
398 aging have not been reported. Our results revealed a novel function of eIF2β to maintain
399 proteostasis during aging.
400
401 How depletion of axonal mitochondria upregulates eIF2β is currently under
402 investigation. A major mitochondrial function is ATP production, and depletion of
403 axonal mitochondria downregulates ATP in axons[33]. However, we found that ATP
404 deprivation did not always suppress autophagy (Figure 3), suggesting it is unlikely to be
405 involved in the mechanisms that induce eIF2β upregulation. Mitochondria also serve as
406 signaling hubs for translation and protein degradation. Mitochondrial proteins are
407 regulated by co-translational protein quality control, and mitochondrial damage induces
408 translational stalling of mitochondrial outer membrane-associated *complex-I 30 kD*
409 *subunit* (*C-I30*) mRNA[43]. Additionally, the mitochondrial outer membrane ubiquitin
410 ligase MITOL (also known as MARCHF5) ubiquitinates and regulates not only
411 mitochondrial proteins such as Mfn2[44] but also microtubule-associated[45] and
412 endoplasmic reticulum[46] proteins. These findings indicate that mitochondria serve as
413 local signaling centers for proteostasis maintenance, and eIF2β levels may also be
414 regulated by mechanisms related to mitochondria.
415
416 In conclusion, our results suggest that axonal mitochondria and eIF2β form an axis to
417 maintain constitutive autophagy. Suppression of *eIF2β* rescued autophagic defects and
418 neuronal dysfunction upon loss of axonal mitochondria. Since eIF2β is conserved across
419 many species, including *Drosophila* and humans, our results suggest that eIF2β may be
420 a possible therapeutic target for aging and diseases associated with mitochondrial
421 mislocalization.
422
423
424 **Materials and methods**
425
426 **Fly stocks and husbandry**
427 Flies were maintained in standard cornmeal medium (10% glucose, 0.7% agar, 9%
428 cornmeal, 4% yeast extract, 0.3% propionic acid, and 0.1% n-butyl p-hydroxybenzoate)
429 at 25°C under light–dark cycles of 12:12 h. The flies were transferred to fresh food vials
430 for every 2–3 days. UAS-*milton* RNAi (v41508) was from VDRC and outcrossed to

431 [w1118] for five generations in our laboratory. Transgenic fly lines carrying
432 UAS-*luciferase* RNAi control for *milton* RNAi) was reported previously[24]. GMR-gal4,
433 Elav-gal4, UAS-*Pfk* RNAi (Bloomington stock center #36782), UAS-*luciferase* RNAi
434 (Bloomington stock center #31603) (control for *Pfk* RNAi), UAS-*GFP* (used for control
435 for UAS-*eIF2β*) and UAS-*eIF2β* (eIF2β^{EY08063}, Bloomington stock center #17425) were
436 from the Bloomington stock center. *eIF2β* heterozygous strain (PBac{SAstopDsRed}
437 LL07719, DGRC#142114) was from KYOTO *Drosophila* Stock Center. UAS-*mitoGFP*
438 was a kind gift from Drs. W. M. Saxton (University of California, Santa Cruz).
439
440 **Immunohistochemistry and image acquisition**
441 Fly brains were dissected in PBS and fixed for 45 minutes in formaldehyde (4% v/v in
442 PBS) at room temperature. After incubation in PBST containing 0.1% Triton X-100 for
443 10 min three times, samples were incubated for 1h at room temperature in PBST
444 containing 1% normal goat serum (Wako, #143-06561) and then incubated overnight
445 with the primary antibody (anti-ubiquitin antibody Ubi-1 (Thermo Fisher #13-1600)
446 (1:50), anti-eIF2α (abcam #ab26197) (1:50) and anti-p-eIF2α (Cell signaling #3398S)
447 (1:50)) diluted in 1% NGS/PBST at 4 °C. Samples were then washed for 10 min with
448 PBST including 0.1% Triton X-100 three times and incubated with the secondary
449 antibody for overnight at 4° C. Brains were mounted in Vectashield (Vectorlab
450 Cat#H-1100) and analyzed under a confocal microscope (Nikon). Quantitative analysis
451 was performed using ImageJ (National Institutes of Health) with maximum projection
452 images derived from Z-stack images acquired with same settings. Puncta were identified
453 with mean intensity and area using ImageJ. For eIF2α and p- eIF2α immunostaining, the
454 mushroom body was detected by mitoGFP expression.
455
456 **Electron microscopy**
457 Proboscis was removed from decapitated heads, which were then incubated in primary
458 fixative solution (2.5% glutaraldehyde and 2% paraformaldehyde in 0.1 M sodium
459 cacodylate buffer) at R.T. for 2 hours. After washing heads with 3% sucrose in 0.1 M
460 sodium cacodylate buffer, fly heads were post-fixed for 1 hour in secondary fixation
461 (1% osmium tetroxide in 0.1 M sodium cacodylate buffer) on ice. After washing with
462 H_2O, heads were dehydrated with ethanol and infiltrated with propylene oxide and Epon
463 mixture (TAAB and Nissin EM) for 3 hours. After infiltration, specimens were
464 embedded with an Epon mixture at 70°C for 2-3 days. Thin sections (70 nm) of laminas
465 were collected on copper grids. The sections were stained with 5% uranyl acetate in

466 50% ethanol and Reynolds' lead citrate solution. Electron micrographs were obtained
467 with a CCD Camera mounted on a JEM-1400 plus electron microscope (Jeol Ltd.).
468 Quantitation was performed using ImageJ (National Institutes of Health).
469
470 **SDS–PAGE and immunoblotting**
471 Western blotting was performed as reported previously[24]. Briefly, heads of 10-20
472 *Drosophila* were homogenized with SDS-Tris-Glycine sample buffer (0.312M Tris, 5%
473 SDS, 8% glycerol, 0.0625% BPB, 10% β-mercaptoethanol, 10μg/mL leupeptin, 0.4 μM
474 Pefabloc, 10mM β-glycerphosphate, 10mM NaF) and after boiling at 95ºC for 2 minutes,
475 it was centrifuged at 13,200 rpm, and the supernatant was used as a sample. For p62
476 western blot, fly heads were homogenized with 1% PBST and after centrifugation at
477 13,200 rpm, the supernatant was mixed 1:1 SDS-Tris-Glycine sample buffer, and boiled
478 at 95 ºC for 2 minutes. The pellet was dissolved with 2% SDS in PBS, then centrifuged
479 again at 13,200 rpm. The supernatant was mixed 1:1 SDS-Tris-Glycine sample buffer
480 and then boiled at 95 ºC for 2 minutes. SDS–PAGE for western blotting was performed
481 using 15%(w/v) (LC3), 7.5%(w/v) (p62), 10% (w/v) (eIF2α, β, and p-eIF2α)
482 polyacrylamide gels. After electrophoresis, they were transferred to PVDF membrane
483 (Merck Millipore) using a transfer device (BIO-RAD). After transfer, the membrane
484 was blocked with 5% skim milk/TBST (50 mM Tris (pH 7.5), 0.15 M NaCl, 0.05%
485 Tween20) for 1 hour and incubated with primary antibody listed below overnight at 4 ºC.
486 Membranes were rinsed twice with TBST containing 0.65M NaCl and once with TBST
487 containing 0.15M NaCl. After incubation with the secondary antibody at room
488 temperature for 1 hour, membranes were rinsed twice with TBST containing 0.65M
489 NaCl and once with TBST containing 0.15M NaCl. After incubation with Immobilon
490 Western Chemiluminescent HRP Substrate (Merck Millipore), chemiluminescent
491 signals were detected with Fusion FX (Vilber). Experiments were repeated at least 3
492 times with independent cohorts of flies.
493 Primary antibodies: anti-LC3 antibody Atg8 (Merck Millipore #ABC975) (1:1000),
494 anti-p62 antibody Ref2P (abcam #ab178440) (1:750), anti-eIF2β antibody (1:1500),
495 anti-eIF2α antibody (abcam #ab26197) (1:1000), anti-p-eIF2α antibody (Cell signaling
496 #3398S) (1:2000), anti-actin antibody (SIGMA A2066) (1:3000) and anti-β tubulin
497 antibody (Sigma #T9026) (1:800,000). Polyclonal anti-eIF2β antibody was raised
498 against a synthetic peptide (CGLEDDTKKEDPQDEA) corresponding to the C-terminal
499 residues 29-43 of *Drosophila* eIF2β (1:1500).
500 Secondary antibodies: Peroxidase-conjugated goat anti-mouse IgG antibody (Dako
501 #P0447) (1:2000), peroxidase-conjugated pig anti-rabbit IgG antibody (Dako #P0399)

502 (1:2000)
503
504 **Proteasome assay**
505 Heads from ten flies were homogenized in 150 µl of buffer B (25 mM Tris-HCl [pH
506 7.5], 2 mM ATP, 5 mM MgCl2, and 1 mM dithiothreitol). Proteasome peptidase activity
507 in the lysates was measured with a synthetic peptide substrate,
508 succinyl-Leu-Leu-Val-Tyr-7-amino-4-methyl-coumarin (Suc-LLVY-AMC) (Cayman).
509 Luminescence was measured on a multimode plate reader 2300 Enspire (PerkinElmer).
510 Experiments were repeated at least 3 times with independent cohorts of flies.
511
512 **ATP assay**
513 Heads from the 10 flies were homogenized in 50 µl of 6 M guanidine-HCl in extraction
514 buffer (100 mM Tris and 4 mM EDTA, pH 7.8) to inhibit ATPases. Samples were boiled
515 for 5 min and centrifuged. The supernatant was diluted 4% with extraction buffer and
516 mixed with a reaction solution (ATP Determination kit, Invitrogen). Luminescence was
517 measured on a multimode plate reader 2300 Enspire (PerkinElmer). The relative ATP
518 levels were calculated by dividing the luminescence by the total protein concentration,
519 which was determined by the Bradford method. Experiments were repeated at least 3
520 times with independent cohorts of flies.
521
522 **Proteomic assay and pathway analysis**
523 *Sample preparation*
524 Heads from the 35 flies were homogenized in 110 µl of extraction buffer (0.25%
525 RapiGest SF, 50mM ammonium bicarbonate, 10mM dithiothreitol, 10µg/mL leupeptin,
526 0.4 µM Pefabloc, 10mM β-glycerphosphate, 10mM NaF). Homogenized samples were
527 centrifuged and boiled for 5 min. After quantification of the protein concentration using
528 a Pierce® 660 nm Protein Assay (Thermo Fisher Scientific), 10 µg proteins from each
529 sample were reduced using 5 mM tris (2-carboxyethyl) phosphine hydrochloride
530 (TCEP-HCl; Thermo Fisher Scientific) at 60°C for 1 h, alkylated using 15 mM
531 iodoacetamide (Fujifilm Wako Pure Chemical, Osaka, Japan) at room temperature for
532 30 min, and then digested using 1.5 µg Trypsin Gold (Mass Spectrometry Grade;
533 Promega, Madison, WI, USA) at 37°C for 17 h. The digests were acidified by the
534 addition of trifluoroacetic acid (TFA), incubated at 37°C for 30 min, and then
535 centrifuged at 17,000 ×*g* for 10 min to remove the RapiGest SF. The supernatants were
536 collected and desalted using MonoSpin™ C18 (GL Sciences, Tokyo, Japan). The
537 resulting eluates were concentrated *in vacuo*, dissolved in 2% MeCN containing 0.1%

538 formic acid (FA), and subjected to LC-MS/MS analysis.
539
540 *LC-MS/MS analysis and database search*
541 LC-MS/MS analyses were performed on an Ultimate 3000 RSLCnano system (Thermo
542 Fisher Scientific) coupled to a Q Exactive hybrid quadrupole-Orbitrap mass
543 spectrometer (Thermo Fisher Scientific) equipped with a nano electron spray ionization
544 (ESI) source. The LC system was equipped with a trap column (C18 PepMap 100, 0.3 ×
545 5 mm, 5 μm, Thermo Fisher Scientific) and an analytical column (NTCC-360/75-3-125,
546 Nikkyo Technos, Tokyo, Japan). Peptide separation was performed using a 90-min
547 gradient of water/0.1% FA (mobile phase A) and MeCN/0.1% FA (mobile phase B) at a
548 flow rate of 300 nL/min. Elution was performed as follows: 0–3 min, 2% B; 3–93 min,
549 2%–40% B; 93–95 min, 40%–95% B; 95–105 min, 95% B; 105–107 min, 95%–2% B;
550 and 107–120 min, 2% B. The mass spectrometer was operated in data-dependent
551 acquisition mode. The MS parameters were as follows: spray voltage, 2.0 kV; capillary
552 temperature, 275°C; S-lens RF level, 50; scan type, full MS; scan range, *m/z* 350–1500;
553 resolution, 70,000; polarity, positive; automatic gain control target, 3×10^6; and
554 maximum injection time, 100 msec. The MS/MS parameters were as follows: resolution,
555 17,500; automatic gain control target, 1×10^5; maximum injection time, 60 msec;
556 normalized collision energy (NCE), 27; dynamic exclusion, 15 sec; loop count, 10;
557 isolation window, 1.6 *m/z*; charge exclusion: unassigned, 1 and ≥8; and injection volume,
558 1 μL (containing 0.5 μg protein). Measurements were made in duplicate for each
559 sample.
560
561 The identification of proteins and label-free quantification (LFQ) of the detected
562 peptides were performed using Proteome Discoverer software ver. 2.4 (Thermo Fisher
563 Scientific). The analytical parameters used for the database search were as follows:
564 parent mass error tolerance, 10.0 ppm; fragment mass error tolerance, 0.02 Da; search
565 engine, sequest HT; protein database, Drosophila melanogaster (Fruit fly: SwissProt Tax
566 ID=7227); enzyme name, trypsin (full); maximum number of missed cleavages, 2;
567 dynamic modification, oxidation (methionine), phosphorylation (serine, threonine,
568 tyrosine), acetyl (lysine), GG (lysine); N-terminal modification, Met-loss (methionine),
569 and Met-loss+acetyl (methionine); static modification, carbamidomethylation (cysteine)
570 and FDR confidence, High < 0.01, 0.01 ≤ Medium < 0.05, 0.05 ≤ Low. The parameters
571 for LFQ were as follows: precursor abundance, based on area; and normalization mode,
572 total peptide amount.
573 The abundance ratio of *milton* RNAi to control RNAi at 7- or 21-day-old was calculated.

574 We considered proteins with an abundance ratio of ≥2.0 or ≤ 0.5 and an ANOVA
575 *P*-value of < 0.05 based on volcano plots to be differentially expressed of *milton* RNAi.
576 To extract molecular networks biologically relevant to the proteins that are differentially
577 expressed in *milton* RNAi, pathway analysis was performed using KeyMolnet (KM
578 Data Inc., Tokyo, Japan).
579
580 **RNA extraction and quantitative real-time PCR analysis**
581 Heads from more than 25 flies were mechanically isolated, and total RNA was extracted
582 using ISOGEN (NipponGene) followed by reverse-transcription using PrimeScript RT
583 reagent kit (Takara). The resulting cDNA was used as a template for PCR with
584 THUNDERBIRD SYBR qPCR mix (TOYOBO) on a Thermal Cycler Dice real-time
585 system TP800 (Takara). Expression of genes of interest was standardized relative to
586 rp49. Relative expression values were determined by the ΔΔCT method (Livak and
587 Schmittgen, 2001). Experiments were repeated three times, and a representative result
588 was shown.
589 Primers were designed using DRSC FlyPrimerBank (Harvard Medical School). Primer
590 sequences are shown below;
591 *eIF2β* for 5′-GGACGACGACAAGAGCGAAG -3′
592 *eIF2β* rev 5′-CGGTCGCATCACGAACTTTG -3′
593 *milton* for 5′-GGCTTCAGGGCCAGGTATCT-3′
594 *milton* rev 5′-GCCGAACTTGGCTGACTTTG-3′
595 *Actin* for 5′-TGCACCGCAAGTGCTTCTAA-3′
596 *Actin* rev 5′-TGCTGCACTCCAAACTTCCA-3′
597 *rp49* for 5′-GCTAAGCTGTCGCACAAATG-3′
598 *rp49* rev 5′- GTTCGATCCGTAACCGATGT-3′
599
600 **Polysome gradient centrifugation**
601 30 heads were homogenized in 150 µl of lysis buffer (25 mM Tris pH 7.5, 50 mM
602 MgCl2, 250 mM NaCl, 1 mM DTT, 0.5 mg/ml cycloheximide, 0.1 mg/ml heparin). The
603 lysates were centrifuged at 13,200 rpm at 4 °C for 5 minutes, and the supernatant was
604 collected. The samples containing 38µg of RNA was layered gently on top of a 10–50%
605 w/w sucrose gradient (50 mM Tris pH 7.5, 50 mM MgCl2, 250 mM NaCl, 0.1 mg/ml
606 heparin, 0.5 mg/ml cycloheximide in 5 ml polyallomer tube) and centrifuged at 37,000
607 rpm at 4°C for 150 minutes in a himac CP-NX ultracentrifuge using a P50AT rotor.
608 Samples were fractionated from top to bottom, and absorbance at OD260 nm was
609 analyzed by a Plate reader (EnSpire). Experiments were repeated at least 3 times with

610 independent cohorts of flies.
611
612 **Puromycin analysis**
613 13-day-old flies were starved for 6 hr and fed 600 μM puromycin (Sigma) or 600 μM
614 puromycin/35 mM cycloheximide (Sigma) in 5% sucrose solution for 20 hr.
615 Incorporated puromycin was quantified by western blot with anti-puromycin antibody
616 and normalized with actin. Experiments were repeated at least 3 times with independent
617 cohorts of flies.
618
619 **Histological analysis**
620 Fly heads were fixed in Bouin's fixative solution for 48 h at room temperature,
621 incubated for 24 h in 50 mM Tris/150 mM NaCl, and embedded in paraffin. Serial
622 sections (7 μm thickness) through the entire heads were stained with hematoxylin and
623 eosin and examined by bright-field microscopy. Images of the sections that include the
624 lamina were captured with Keyence microscope BZ-X700 (Keyence), and the vacuole
625 area was measured using ImageJ (National Institutes of Health).
626
627 **Climbing assay**
628 The climbing assay was performed as previously described[24]. Flies were placed in an
629 empty plastic vial (2.5 cm in diameter × 10 cm in length). The vial was gently tapped to
630 knock the flies to the bottom, and the number of flies reached to the top, middle and
631 bottom areas of the vials in 10 s was counted. Experiments were repeated 10 times, and
632 the mean percentage of flies in each area and standard deviations were calculated.
633 Experiments were repeated with independent cohorts more than three times, and a
634 representative result was shown.
635
636 **Statistics**
637 The number of replicates, what n represents, precision measurements, and the meaning
638 of error bars are indicated in Figure Legends. Data are shown as means ± SEM. For
639 pairwise comparisons, Student's t-test was performed with Microsoft Excel (Microsoft).
640 For multiple comparisons, data were analyzed using one-way ANOVA with Tukey's
641 HSD multiple-comparisons test in the GraphPad Prism 6.0 software (GraphPad
642 Software, Inc., La Jolla, CA). Results with a p-value of less than 0.05 were considered
643 to be statistically significant.
644
645

Acknowledgments

The authors thank the Bloomington stock center; TRiP at Harvard Medical School (NIH/NIGMS R01-GM084947); the Kyoto Drosophila Stock Center and the Vienna Drosophila RNAi Center for fly stocks. The authors thank Dr. Masayuki Miura from Department of Pharmaceutical Science, University of Tokyo, for proteasome activity assay protocol; Dr. Shin-ichi Hisanaga from the Department of Biological Sciences, Tokyo Metropolitan University, for critical comments; Dr. Taro Saito, Dr. Akiko Asada from the Department of Biological Sciences, Tokyo Metropolitan University, Dr. Michiko Sekiya from Department of Alzheimer's Disease Research, National Center for Geriatrics and Gerontology, and Dr. Seiji Watanabe, Dr. Koji Yamanaka from Department of Neuroscience and Pathobiology, Research Institute of Environmental Medicine, Nagoya University for technical supports.

Funding

This work was supported by the Sasakawa Scientific Research Grant (2021-4087) (to K.S.), the Takeda Science Foundation (to KA), Hoansha foundation grant (to KA), a research award from the Japan Foundation for Aging and Health (to KA), the Novartis Foundation (Japan) for the promotion of Science (to KA), JSPS KAKENHI Grant-in-Aid for Scientific Research on Challenging Research (Exploratory) JP19K21593 (to KA), JSPS KAKENHI Grant-in-Aid for Scientific Research(B) JP24K02860 (to KA), NIG-JOINT (National Institute of Genetics, 71A2018, 25A2019) (to K.A.) and TMU strategic research fund for social engagement (to KA).

Author contributions

K.S. and K.A. designed the experiments, interpreted the data, and wrote the manuscript; K.S., Y.M., K.M.I and E.S. conducted the experiments, and K.S., Y.M., E.S., and K.A. analyzed the data. All authors read and approved the manuscript.

Declaration of interests

The authors declare no competing interests.

Data Availability

The datasets used and/or analyzed during the current study are available from the

682 corresponding author upon request.
683
684
685 **Figure legends**
686
687
688 **Figure 1. Knockdown of *milton* or *Miro* causes protein accumulation in the axon**
689 (A) Schematic representation of the mitochondrial transport machinery. Knockdown of
690 *milton*, an adapter protein for mitochondrial transport, depletes mitochondria in the axon.
691 (B, C) Ubiquitinated proteins in brains with neuronal knockdown of *milton* or *Miro*.
692 Brains dissected at 14-day-old (B) or 30-day-old (C) were immunostained with an
693 antibody against ubiquitin. Firefly *luciferase* RNAi was used as a control.
694 Representative images (left) and quantitation of the number of ubiquitin-positive puncta
695 (right) are shown. Scale bars of hemibrains, 100 μm, Scale bars of high magnifications,
696 10 μm. Means ± SE, n = 8. *N.S.*, $p > 0.05$; ***$p < 0.005$ (one-way analysis of variance
697 (ANOVA) followed by Tukey's honestly significant difference (HSD) *post hoc* test). (D)
698 Cross sections in the lamina and in the retina were used to analyze the ultrastructure of
699 synapses and cell bodies, respectively. *milton* RNAi was expressed in the retina and
700 neurons via a combination of GAL4 drivers, a pan-retinal gmr-GAL4 and pan-neuronal
701 elav-GAL4. (E) Quantitation of the number of mitochondria in a presynaptic terminal
702 from transmission electron micrographs. 180 presynaptic terminals from cross-sections
703 of the lamina from three brains were analyzed. ***$p < 0.005$ (Chi-square test). (F, G)
704 Presynaptic terminals of photoreceptor neurons of control and *milton* knockdown flies.
705 Photoreceptor neurons are highlighted in blue. Swollen presynaptic terminals (asterisks
706 in (F)), characterized by the enlargement and higher circularity, were found more
707 frequently in *milton* knockdown neurons. Arrowheads indicate presynaptic terminals
708 with dense materials. Scale bars, 2 μm. Representative images (Left) and quantitation
709 (Right) are shown. 918–1118 from three heads were quantified for the percentage of
710 swollen presynaptic terminals, and 180 presynaptic terminals from three heads were
711 quantified for the size of presynaptic terminals. Mean ± SE, **$p < 0.01$, ***$p < 0.005$
712 (Student's *t*-test). (G) Dense materials (arrowheads in (G)) in the presynaptic terminals
713 of *milton* knockdown neurons. Scale bars, 2 μm. The ratio of presynaptic terminals
714 containing dense materials were quantified from 918–1118 presynaptic terminals from
715 three heads. Mean ± SE, ***$p < 0.005$ (Student's *t*-test). (H) Cell bodies of
716 photoreceptor neurons of control and *milton* knockdown flies. Scale bars, 2 μm. Flies
717 were 27-day-old.

718

719 **Figure 2. *milton* knockdown impairs protein degradation pathways**

720 (A, B) Western blotting of head extracts of control and *milton* knockdown flies with
721 antibodies against LC3 (A) and Ref2P, the fly homolog of mammalian p62 (B). For the
722 analyses of p62 levels, heads were extracted with 1% Triton X-100 or 2% SDS (B).
723 Flies were 14-day-old. Representative blots (left) and quantitation (right) are shown.
724 Actin was used as a loading control. Means ± SE, n = 6 (LC3), n = 3 (p62). (C)
725 Proteasome activity in head extracts of control and *milton* knockdown flies was
726 measured by hydrolysis of Suc-LLVY-AMC at 14-day-old. Means ± SE, n = 3. (D, E)
727 Western blotting of head extracts of 30-day-old control and *milton* knockdown flies.
728 Blotting was performed with anti-LC3 (D) and anti-p62 (E) antibodies. Representative
729 blots (left) and quantitation (right) are shown. Actin was used as a loading control.
730 Means ± SE, n = 6 (LC3), n = 3 (p62). (F) Proteasome activity in head extracts of
731 30-day-old control and *milton* knockdown flies. Means ± SE, n = 3. *N.S.*, $p > 0.05$; *$p <$
732 0.05; **$p < 0.01$; ***$p < 0.005$ (Student's *t*-test).

733

734 **Figure 3. ATP deprivation does not impair autophagy**

735 (A-C) ATP levels in brain extracts of control and *milton* knockdown flies (A) and
736 control and *Pfk* knockdown flies (B) and comparison of the effects of *milton*
737 knockdown and *Pfk* knockdown on ATP levels (C). Flies were 14-day-old. Means ± SE,
738 n = 3. (D, E) Western blotting of head extracts of flies with neuronal expression of
739 control or *Pfk* RNAi. Blotting was performed with anti-LC3 (D) and anti-p62 (E)
740 antibodies. For analyses of p62 levels, heads were extracted with 1% Triton X-100 or
741 2% SDS. Representative blots (left) and quantitation (right) are shown. Actin was used
742 as a loading control. Means ± SE, n = 6 (LC3), n = 3 (p62). (F) Proteasome activity in
743 head lysates of flies with neuronal expression of control or *Pfk* RNAi was measured by
744 hydrolysis of Suc-LLVY-AMC. Means ± SE, n = 3. *N.S.*, $p > 0.05$; *$p < 0.05$; **$p <$
745 0.01; ***$p < 0.005$ (Student's *t*-test). Flies were at 14-day-old.

746

747 **Figure 4. *milton* knockdown upregulates eIF2β in young flies**

748 (A) Timing of proteome analysis and phenotypes observed in *milton* knockdown flies.
749 (B, C) Scatter plots of the $\log_2$ abundance ratio (x-axis) against the $-\log_{10}$ p-value
750 (y-axis) of proteins at 7-day-old (B) and 21-day-old (C). (D) eIF2 subunit protein levels
751 from proteome analysis of *milton* knockdown flies compared to those of control flies.
752 (E) Western blotting of head extracts of flies expressing control or *milton* RNAi in
753 neurons with an anti-eIF2β antibody. Flies were 14-day-old. Representative blots (left)

754 and quantitation (right) are shown. Tubulin was used as a loading control. Means ± SE,
755 n = 6. (F) *eIF2β* mRNA levels quantified by qRT-PCR. Means ± SE, n = 4. (G) Western
756 blotting of head extracts of wild-type flies with an anti-eIF2β antibody. Flies were 7-,
757 21-, 35-, 49- and 63-day-old. Representative blots (left) and quantitation (right) are
758 shown. Tubulin was used as a loading control. Means ± SE, n = 3, $*p < 0.05$ (one-way
759 analysis of variance (ANOVA) followed by Dunnett's multiple comparison test).
760
761 **Figure 5. *milton* knockdown decreases phosphorylation of eIF2α**
762 (A, B) Western blotting of head extracts with anti-eIF2α (A) and anti-p-eIF2α (B)
763 antibodies. Flies were 14-day-old. Representative blots (left) and quantitation (right) are
764 shown. Tubulin was used as a loading control. Means ± SE, n = 6. (C) A schematic
765 representation of the axon (Lobe tips), the cell body region (Kenyon cells), and
766 dendritic region (Calyxes) in the fly brain. Scale bars, 100μm. (D, E) Immunostaining
767 with anti-eIF2α and anti-p-eIF2α antibodies. The mushroom body was identified by
768 expression of mito-GFP. Scale bars, 20μm. The signal intensities of eIF2α and p-eIF2α
769 in axons, dendrites, and cell bodies were quantified and are shown as ratios relative to
770 the control. Means ± SE, n=12. *N.S.*, $p > 0.05$; $*p < 0.05$; $**p < 0.01$; $***p < 0.005$
771 (Student's *t*-test).
772
773 **Figure 6. *milton* knockdown suppressed global translation**
774 (A) Representative polysome traces of head lysates of control and *milton* knockdown
775 flies. (B) Quantitation of polysome fraction. The relative ratio of area under the curve
776 (AUC) of polysome fractions (sedimentation 28%-50%). Means ± SE, n = 3. $***p <$
777 0.005 (Student's *t*-test) (C) Western blotting of head lysates of control and *milton*
778 knockdown flies fed puromycin alone or puromycin and cycloheximide (CHX) with an
779 anti-puromycin antibody. Flies were 14-day-old. Actin was used as a loading control.
780 Representative blots (left) and quantitation (right) are shown. Means ± SE, n = 3.
781 Student's *t*-test.
782
783 **Figure 7. eIF2β upregulation impairs autophagy and decreases locomotor function**
784 (A) *eIF2β* mRNA levels in head extracts of flies with UAS-*eIF2β* driven by elav-Gal4
785 (*eIF2β* OE) or UAS-GFP driven by elav-Gal4 (control) were quantified by qRT-PCR.
786 Flies were 2-day-old. Means ± SE, n=4. (B, C) Western blotting of head extracts with
787 anti-LC3 (B) and anti-p62 (C) antibodies. Flies were 14-day-old. Representative blots
788 (left) and quantitation (right) are shown. Tubulin and actin were used as loading
789 controls. Means ± SE, n = 3 (p62), n = 5 (LC3). (D, E) Western blotting of head extracts

790 with anti-eIF2α (D) and anti-p-eIF2α (E) antibodies. Flies were 14-day-old.
791 Representative blots (left) and quantitation (right) are shown. Tubulin was used as a
792 loading control. Means ± SE, n = 6. (F) Climbing assay revealed early-onset of
793 age-dependent locomotor defects in *eIF2β*-overexpressing flies. Means ± SE, n = 5.
794 *N.S.*, $p > 0.05$; ***$p < 0.005$ (Student's *t*-test).
795
796 **Figure 8. Lowering *eIF2β* rescues autophagic impairment and locomotor**
797 **dysfunction induced by *milton* knockdown**
798 (A) *eIF2β* mRNA levels with one disrupted copy of the *eIF2β* gene
799 (*eIF2β*SAstopDsRed/+ (*eIF2β* -/+)). Head extracts of flies 2-3 day-old were analyzed
800 by qRT-PCR. Means ± SE, n = 3. (B, C) Western blotting of head extracts of flies with
801 neuronal expression of *milton* RNAi with or without *eIF2β* heterozygosity with
802 anti-LC3 (B) and anti-p62 (C) antibodies. Flies were 14-day-old. Representative blots
803 (left) and quantitation (right) are shown. Actin was used as a loading control. Means ±
804 SE, n = 5 (LC3), n = 3 (p62). (D) The climbing ability of 20-day-old flies expressing
805 *milton* RNAi with or without *eIF2β* heterozygosity. Means ± SE, n = 15. *N.S.*, $p > 0.05$;
806 *$p < 0.05$; ***$p < 0.005$ (Student's *t*-test).
807
808 **Figure 9. Graphical abstract: the mitochondria-eIF2β axis in the axon maintains**
809 **neuronal proteostasis during aging**
810
811
812 **Supplemental Figure 1. Ubiquitinated proteins in brains with neuronal knockdown**
813 **of *milton* at 1-day-old**
814 Brains dissected at 1-day-old were immunostained with an antibody against ubiquitin.
815 Representative images (left) and quantitation of the number of ubiquitin-positive puncta
816 (right) are shown. Scale bars of hemibrains, 100 μm, Means ± SE, n = 8. *N.S.*, $p > 0.05$
817 (Student's *t*-test).
818
819 **Supplemental Figure 2. Histology analysis of fly heads with *eIF2β* overexpression**
820 The morphology of the eye with eIF2β overexpression. The dotted lines indicate the
821 retina. Vacuoles are indicated by arrows. Representative images (left) and quantification
822 of vacuole area (right). The flies were 40-day-old. Means ± SE, n = 5-13 *N.S.*, $p > 0.05$
823 (Student's *t*-test).
824
825 **Supplemental Figure 3. Lowering the eIF2β level does not affect the levels of eIF2α**

and p-eIF2α.

(A, B) Blotting was performed with anti-eIF2α (A) and anti-p-eIF2α (B) antibodies. Flies were 14-day-old. Representative blots (left) and quantitation (right) are shown. Tubulin was used as a loading control. Means ± SE, n = 6. (C) *eIF2β* gene disruption does not affect the knockdown efficiency of *milton*. *milton* mRNA levels in head extracts were quantified by qRT-PCR. Flies were 2-day-old. Means ± SE, n = 3. *N.S.*, $p > 0.05$; $*p < 0.05$ (Student's *t*-test).

References

1. Yerbury, J.J., Ooi, L., Dillin, A., Saunders, D.N., Hatters, D.M., Beart, P.M., Cashman, N.R., Wilson, M.R., and Ecroyd, H. (2016). Walking the tightrope: proteostasis and neurodegenerative disease. J. Neurochem. *137*, 489-505. 10.1111/jnc.13575.
2. Hetz, C. (2021). Adapting the proteostasis capacity to sustain brain healthspan. Cell *184*, 1545-1560. 10.1016/j.cell.2021.02.007.
3. Balch, W.E., Morimoto, R.I., Dillin, A., and Kelly, J.W. (2008). Adapting proteostasis for disease intervention. Science *319*, 916-919. 10.1126/science.1141448.
4. Kimball, S.R. (1999). Eukaryotic initiation factor eIF2. Int J Biochem Cell Biol *31*, 25-29. 10.1016/s1357-2725(98)00128-9.
5. Jackson, R.J., Hellen, C.U., and Pestova, T.V. (2010). The mechanism of eukaryotic translation initiation and principles of its regulation. Nat. Rev. Mol. Cell Biol. *11*, 113-127. 10.1038/nrm2838.
6. Pakos-Zebrucka, K., Koryga, I., Mnich, K., Ljujic, M., Samali, A., and Gorman, A.M. (2016). The integrated stress response. EMBO Rep *17*, 1374-1395. 10.15252/embr.201642195.
7. Kroemer, G., Marino, G., and Levine, B. (2010). Autophagy and the integrated stress response. Mol. Cell *40*, 280-293. 10.1016/j.molcel.2010.09.023.
8. Nandi, D., Tahiliani, P., Kumar, A., and Chandu, D. (2006). The ubiquitin-proteasome system. J Biosci *31*, 137-155. 10.1007/BF02705243.
9. Glick, D., Barth, S., and Macleod, K.F. (2010). Autophagy: cellular and molecular mechanisms. J. Pathol. *221*, 3-12. 10.1002/path.2697.
10. Vargas, J.N.S., Hamasaki, M., Kawabata, T., Youle, R.J., and Yoshimori, T. (2023). The mechanisms and roles of selective autophagy in mammals. Nat. Rev. Mol. Cell

862 Biol. *24*, 167-185. 10.1038/s41580-022-00542-2.
863 11. Aman, Y., Schmauck-Medina, T., Hansen, M., Morimoto, R.I., Simon, A.K., Bjedov,
864 I., Palikaras, K., Simonsen, A., Johansen, T., Tavernarakis, N., et al. (2021).
865 Autophagy in healthy aging and disease. Nat Aging *1*, 634-650.
866 10.1038/s43587-021-00098-4.
867 12. Ross, C.A., and Poirier, M.A. (2004). Protein aggregation and neurodegenerative
868 disease. Nat. Med. *10 Suppl*, S10-17. 10.1038/nm1066.
869 13. Rubinsztein, D.C., Marino, G., and Kroemer, G. (2011). Autophagy and aging. Cell
870 *146*, 682-695. 10.1016/j.cell.2011.07.030.
871 14. Vos, M., Lauwers, E., and Verstreken, P. (2010). Synaptic mitochondria in synaptic
872 transmission and organization of vesicle pools in health and disease. Front
873 Synaptic Neurosci *2*, 139. 10.3389/fnsyn.2010.00139.
874 15. Cheng, A., Hou, Y., and Mattson, M.P. (2010). Mitochondria and neuroplasticity.
875 ASN Neuro *2*, e00045. 10.1042/AN20100019.
876 16. Hollenbeck, P.J., and Saxton, W.M. (2005). The axonal transport of mitochondria.
877 J. Cell Sci. *118*, 5411-5419. 10.1242/jcs.02745.
878 17. Takihara, Y., Inatani, M., Eto, K., Inoue, T., Kreymerman, A., Miyake, S., Ueno,
879 S., Nagaya, M., Nakanishi, A., Iwao, K., et al. (2015). In vivo imaging of axonal
880 transport of mitochondria in the diseased and aged mammalian CNS. Proc Natl Acad
881 Sci U S A *112*, 10515-10520. 10.1073/pnas.1509879112.
882 18. Milde, S., Adalbert, R., Elaman, M.H., and Coleman, M.P. (2015). Axonal transport
883 declines with age in two distinct phases separated by a period of relative stability.
884 Neurobiol. Aging *36*, 971-981. 10.1016/j.neurobiolaging.2014.09.018.
885 19. Vagnoni, A., Hoffmann, P.C., and Bullock, S.L. (2016). Reducing Lissencephaly-1
886 levels augments mitochondrial transport and has a protective effect in adult
887 Drosophila neurons. J. Cell Sci. *129*, 178-190. 10.1242/jcs.179184.
888 20. Morsci, N.S., Hall, D.H., Driscoll, M., and Sheng, Z.H. (2016). Age-Related Phasic
889 Patterns of Mitochondrial Maintenance in Adult Caenorhabditis elegans Neurons.
890 J. Neurosci. *36*, 1373-1385. 10.1523/JNEUROSCI.2799-15.2016.
891 21. Adalbert, R., and Coleman, M.P. (2013). Review: Axon pathology in age-related
892 neurodegenerative disorders. Neuropathol. Appl. Neurobiol. *39*, 90-108.
893 10.1111/j.1365-2990.2012.01308.x.
894 22. Duncan, J.E., and Goldstein, L.S. (2006). The genetics of axonal transport and
895 axonal transport disorders. PLoS Genet. *2*, e124. 10.1371/journal.pgen.0020124.
896 23. Chen, H., and Chan, D.C. (2009). Mitochondrial dynamics--fusion, fission, movement,
897 and mitophagy--in neurodegenerative diseases. Hum. Mol. Genet. *18*, R169-176.

898 10.1093/hmg/ddp326.
899 24. Iijima-Ando, K., Sekiya, M., Maruko-Otake, A., Ohtake, Y., Suzuki, E., Lu, B.,
900 and Iijima, K.M. (2012). Loss of axonal mitochondria promotes tau-mediated
901 neurodegeneration and Alzheimer's disease-related tau phosphorylation via PAR-1.
902 PLoS Genet. *8*, e1002918. 10.1371/journal.pgen.1002918.
903 25. Lopez-Domenech, G., Higgs, N.F., Vaccaro, V., Ros, H., Arancibia-Carcamo, I.L.,
904 MacAskill, A.F., and Kittler, J.T. (2016). Loss of Dendritic Complexity Precedes
905 Neurodegeneration in a Mouse Model with Disrupted Mitochondrial Distribution in
906 Mature Dendrites. Cell Rep *17*, 317-327. 10.1016/j.celrep.2016.09.004.
907 26. Guo, X., Macleod, G.T., Wellington, A., Hu, F., Panchumarthi, S., Schoenfield,
908 M., Marin, L., Charlton, M.P., Atwood, H.L., and Zinsmaier, K.E. (2005). The GTPase
909 dMiro is required for axonal transport of mitochondria to Drosophila synapses.
910 Neuron *47*, 379-393. 10.1016/j.neuron.2005.06.027.
911 27. Glater, E.E., Megeath, L.J., Stowers, R.S., and Schwarz, T.L. (2006). Axonal
912 transport of mitochondria requires milton to recruit kinesin heavy chain and is
913 light chain independent. J. Cell Biol. *173*, 545-557. 10.1083/jcb.200601067.
914 28. Stowers, R.S., Megeath, L.J., Gorska-Andrzejak, J., Meinertzhagen, I.A., and
915 Schwarz, T.L. (2002). Axonal transport of mitochondria to synapses depends on
916 milton, a novel Drosophila protein. Neuron *36*, 1063-1077.
917 10.1016/s0896-6273(02)01094-2.
918 29. Iijima-Ando, K., Hearn, S.A., Shenton, C., Gatt, A., Zhao, L., and Iijima, K. (2009).
919 Mitochondrial mislocalization underlies Abeta42-induced neuronal dysfunction in
920 a Drosophila model of Alzheimer's disease. PLoS One *4*, e8310.
921 10.1371/journal.pone.0008310.
922 30. Tonoki, A., Kuranaga, E., Tomioka, T., Hamazaki, J., Murata, S., Tanaka, K., and
923 Miura, M. (2009). Genetic evidence linking age-dependent attenuation of the 26S
924 proteasome with the aging process. Mol. Cell. Biol. *29*, 1095-1106.
925 10.1128/MCB.01227-08.
926 31. Klionsky, D.J., Abdel-Aziz, A.K., Abdelfatah, S., Abdellatif, M., Abdoli, A., Abel,
927 S., Abeliovich, H., Abildgaard, M.H., Abudu, Y.P., Acevedo-Arozena, A., et al.
928 (2021). Guidelines for the use and interpretation of assays for monitoring
929 autophagy (4th edition)(1). Autophagy *17*, 1-382. 10.1080/15548627.2020.1797280.
930 32. Bartlett, B.J., Isakson, P., Lewerenz, J., Sanchez, H., Kotzebue, R.W., Cumming,
931 R.C., Harris, G.L., Nezis, I.P., Schubert, D.R., Simonsen, A., and Finley, K.D.
932 (2011). p62, Ref(2)P and ubiquitinated proteins are conserved markers of neuronal
933 aging, aggregate formation and progressive autophagic defects. Autophagy *7*,

934 572-583. 10.4161/auto.7.6.14943.
935 33. Oka, M., Suzuki, E., Asada, A., Saito, T., Iijima, K.M., and Ando, K. (2021).
936 Increasing neuronal glucose uptake attenuates brain aging and promotes life span
937 under dietary restriction in Drosophila. iScience *24*, 101979.
938 10.1016/j.isci.2020.101979.
939 34. Zia, A., Pourbagher-Shahri, A.M., Farkhondeh, T., and Samarghandian, S. (2021).
940 Molecular and cellular pathways contributing to brain aging. Behav Brain Funct
941 *17*, 6. 10.1186/s12993-021-00179-9.
942 35. Haigis, M.C., and Yankner, B.A. (2010). The aging stress response. Mol. Cell *40*,
943 333-344. 10.1016/j.molcel.2010.10.002.
944 36. Wek, R.C. (2018). Role of eIF2alpha Kinases in Translational Control and Adaptation
945 to Cellular Stress. Cold Spring Harb Perspect Biol *10*.
946 10.1101/cshperspect.a032870.
947 37. Currais, A., Fischer, W., Maher, P., and Schubert, D. (2017). Intraneuronal protein
948 aggregation as a trigger for inflammation and neurodegeneration in the aging brain.
949 FASEB J. *31*, 5-10. 10.1096/fj.201601184.
950 38. Grimm, A., and Eckert, A. (2017). Brain aging and neurodegeneration: from a
951 mitochondrial point of view. J. Neurochem. *143*, 418-431. 10.1111/jnc.14037.
952 39. Bond, S., Lopez-Lloreda, C., Gannon, P.J., Akay-Espinoza, C., and Jordan-Sciutto,
953 K.L. (2020). The Integrated Stress Response and Phosphorylated Eukaryotic
954 Initiation Factor 2alpha in Neurodegeneration. J. Neuropathol. Exp. Neurol. *79*,
955 123-143. 10.1093/jnen/nlz129.
956 40. B'Chir, W., Maurin, A.C., Carraro, V., Averous, J., Jousse, C., Muranishi, Y.,
957 Parry, L., Stepien, G., Fafournoux, P., and Bruhat, A. (2013). The eIF2alpha/ATF4
958 pathway is essential for stress-induced autophagy gene expression. Nucleic Acids
959 Res. *41*, 7683-7699. 10.1093/nar/gkt563.
960 41. Salton, G.D., Laurino, C., Mega, N.O., Delgado-Canedo, A., Setterblad, N.,
961 Carmagnat, M., Xavier, R.M., Cirne-Lima, E., Lenz, G., Henriques, J.A.P., and
962 Laurino, J.P. (2017). Deletion of eIF2beta lysine stretches creates a dominant
963 negative that affects the translation and proliferation in human cell line: A tool
964 for arresting the cell growth. Cancer Biol Ther *18*, 560-570.
965 10.1080/15384047.2017.1345383.
966 42. Lee, S., Nahm, M., Lee, M., Kwon, M., Kim, E., Zadeh, A.D., Cao, H., Kim, H.J.,
967 Lee, Z.H., Oh, S.B., et al. (2007). The F-actin-microtubule crosslinker Shot is
968 a platform for Krasavietz-mediated translational regulation of midline axon
969 repulsion. Development *134*, 1767-1777. 10.1242/dev.02842.

970 43. Wu, Z., Tantray, I., Lim, J., Chen, S., Li, Y., Davis, Z., Sitron, C., Dong, J.,
971 Gispert, S., Auburger, G., et al. (2019). MISTERMINATE Mechanistically Links
972 Mitochondrial Dysfunction with Proteostasis Failure. Mol. Cell *75*, 835-848 e838.
973 10.1016/j.molcel.2019.06.031.
974 44. Sugiura, A., Nagashima, S., Tokuyama, T., Amo, T., Matsuki, Y., Ishido, S., Kudo,
975 Y., McBride, H.M., Fukuda, T., Matsushita, N., et al. (2013). MITOL regulates
976 endoplasmic reticulum-mitochondria contacts via Mitofusin2. Mol. Cell *51*, 20-34.
977 10.1016/j.molcel.2013.04.023.
978 45. Yonashiro, R., Kimijima, Y., Shimura, T., Kawaguchi, K., Fukuda, T., Inatome, R.,
979 and Yanagi, S. (2012). Mitochondrial ubiquitin ligase MITOL blocks S-nitrosylated
980 MAP1B-light chain 1-mediated mitochondrial dysfunction and neuronal cell death.
981 Proc Natl Acad Sci U S A *109*, 2382-2387. 10.1073/pnas.1114985109.
982 46. Takeda, K., Nagashima, S., Shiiba, I., Uda, A., Tokuyama, T., Ito, N., Fukuda,
983 T., Matsushita, N., Ishido, S., Iwawaki, T., et al. (2019). MITOL prevents ER
984 stress-induced apoptosis by IRE1alpha ubiquitylation at ER-mitochondria contact
985 sites. EMBO J. *38*, e100999. 10.15252/embj.2018100999.
986

Shinno et. al., Figure 1

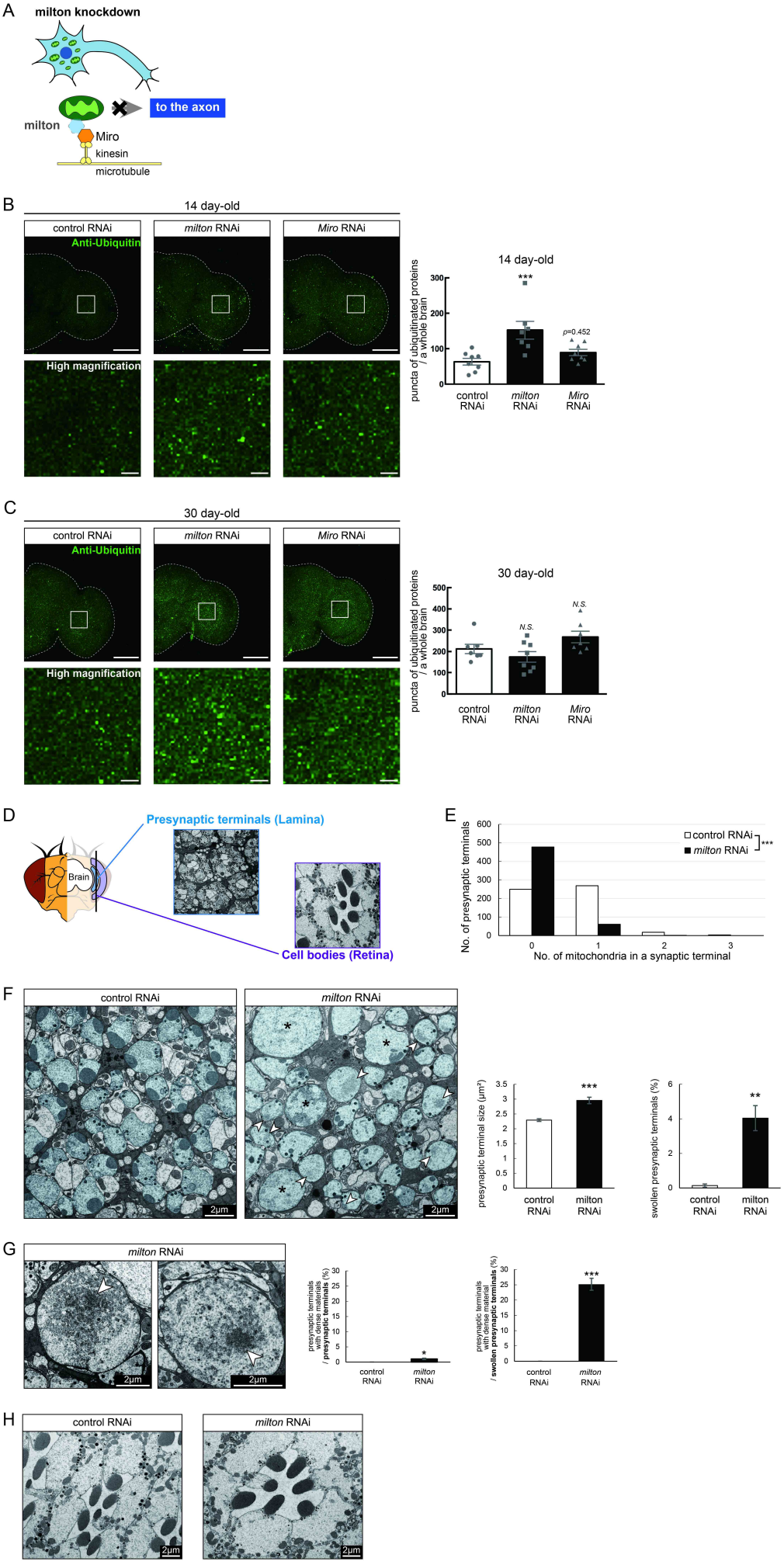

Shinno et. al., Figure 2

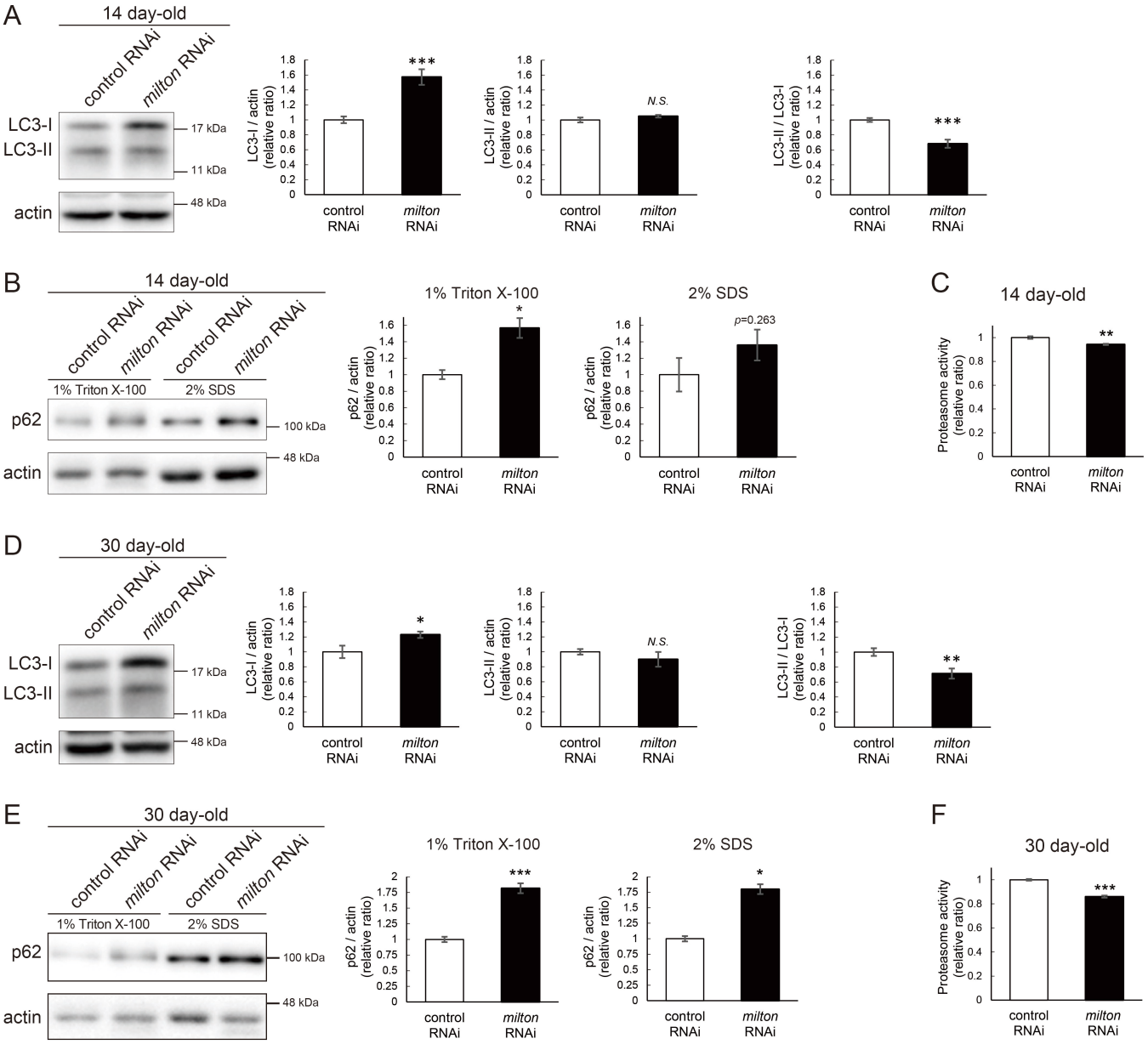

Shinno et. al., Figure 3

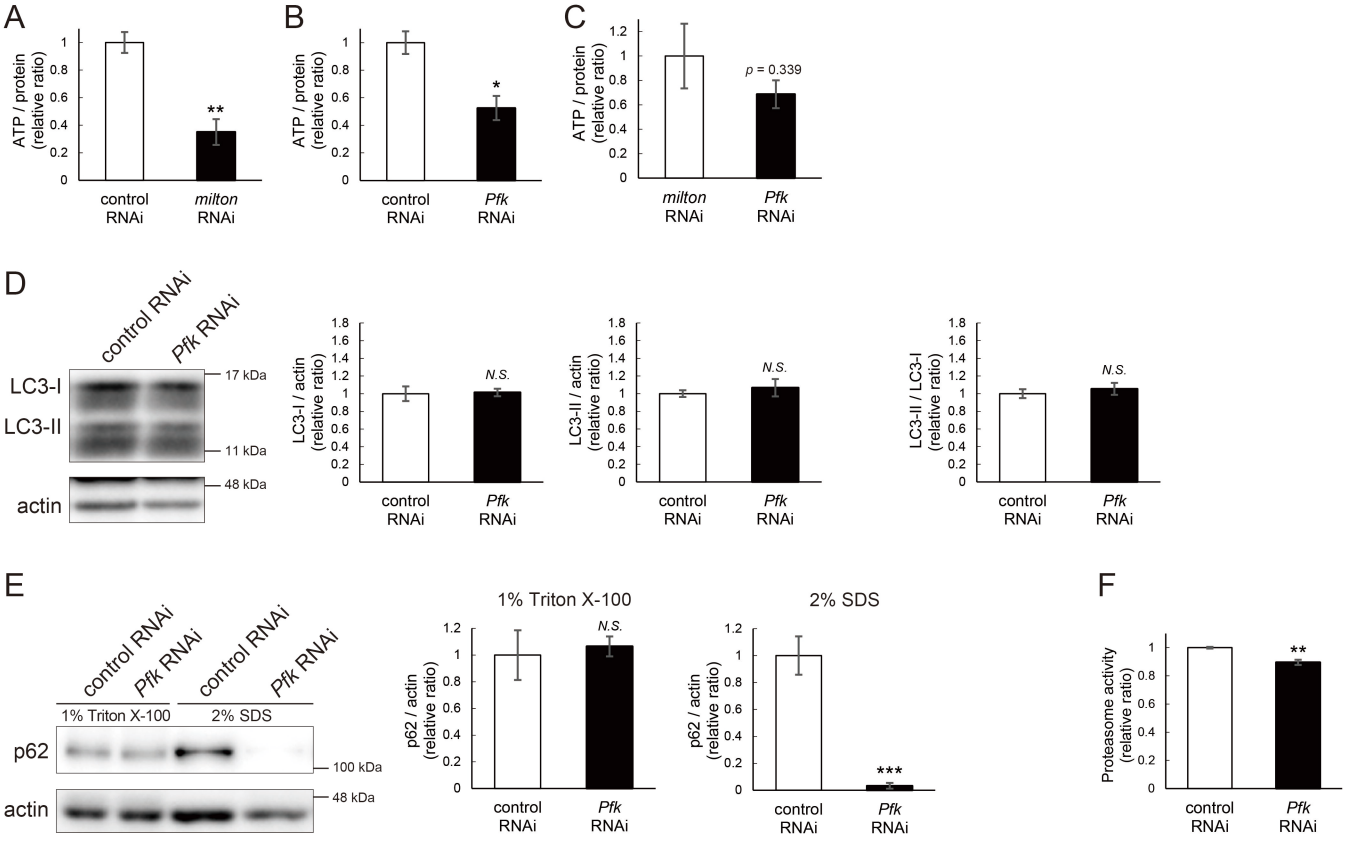

Shinno et. al., Figure 5

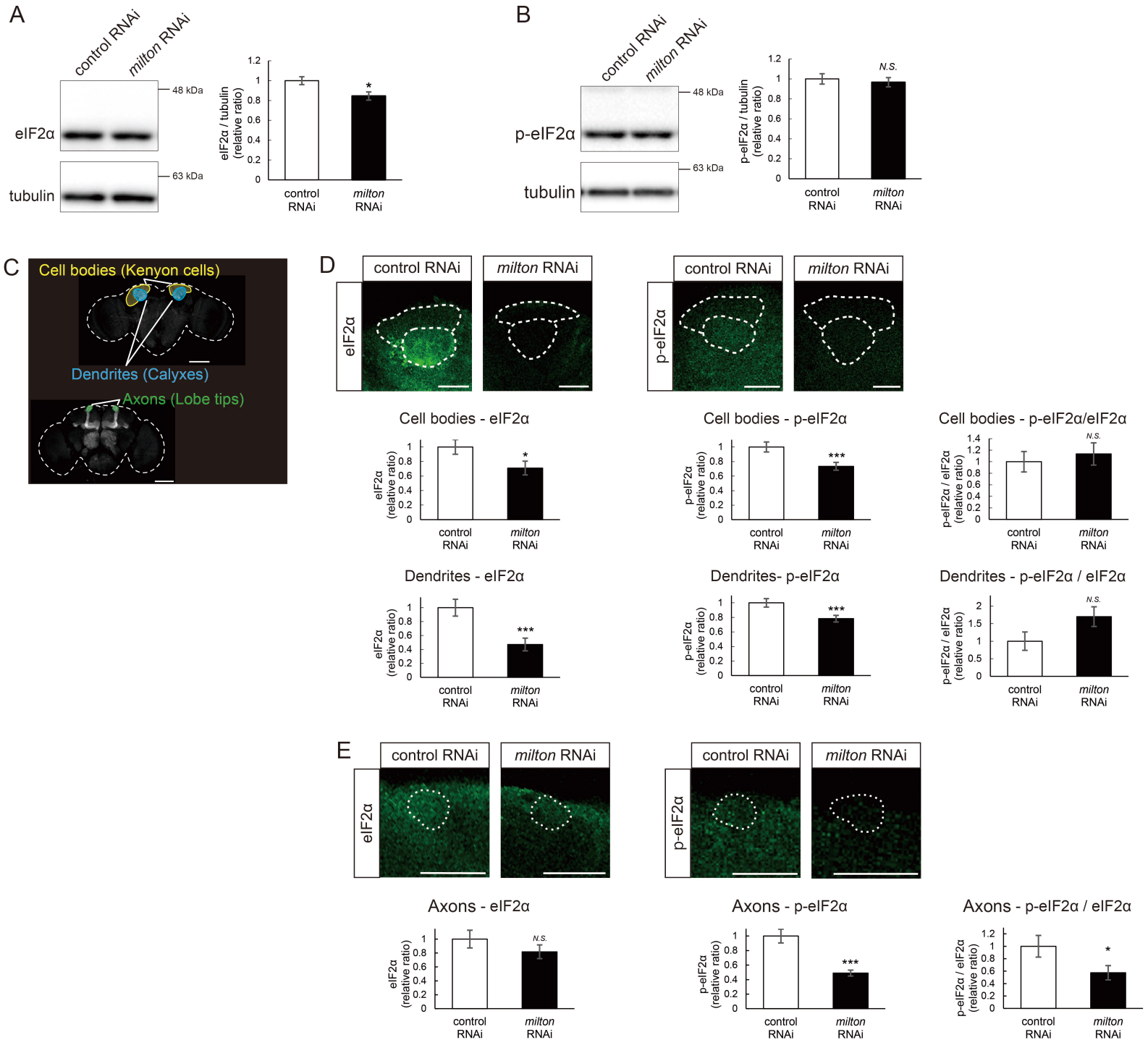

Shinno et. al., Figure 4

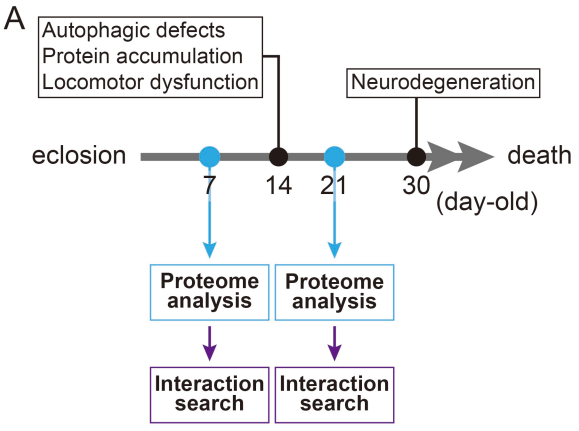

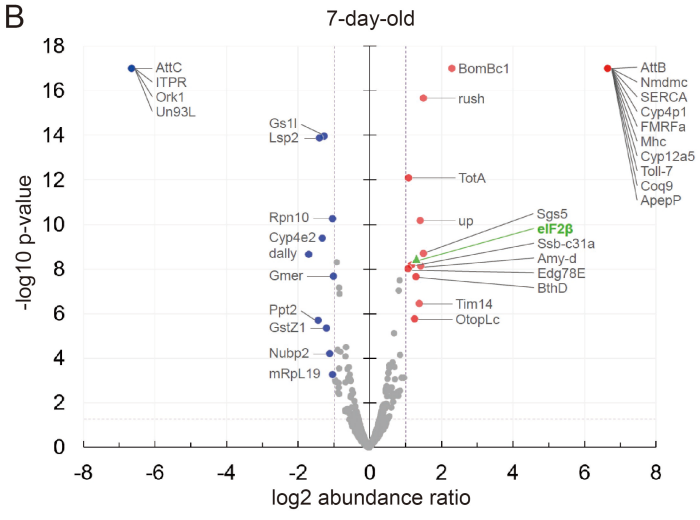

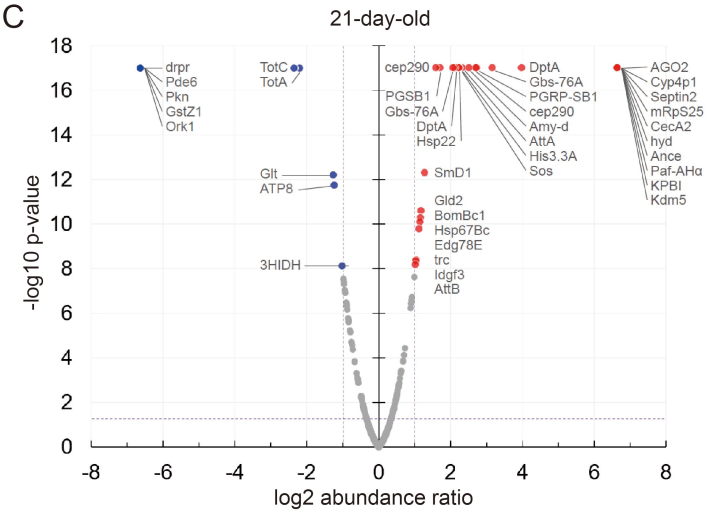

D

		Abundance Ratio : *milton* RNAi / control RNAi	
	Accession	7-day-old	21-day-old
eIF2α	P41374	1.106	0.961
eIF2β	P41375	2.465***	0.753*
eIF2γ	Q24208	0.952	0.952

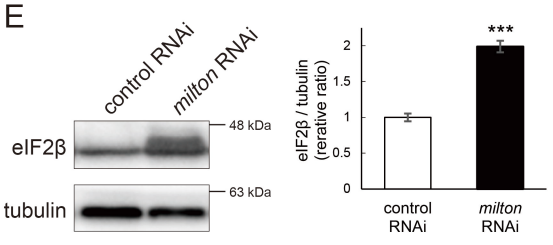

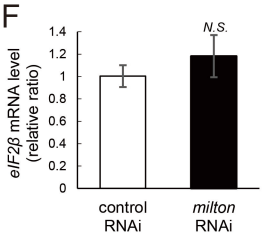

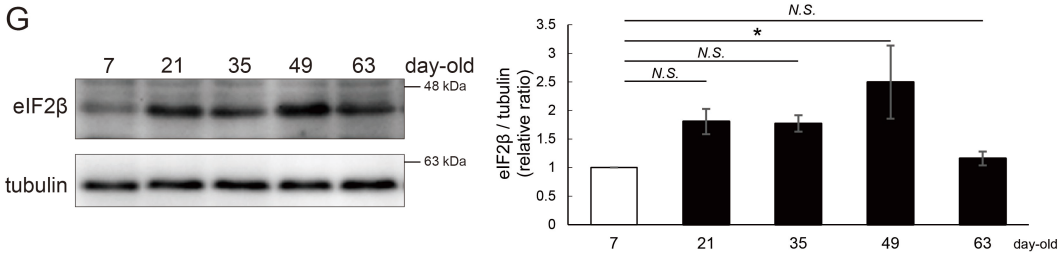

Shinno et. al., Figure 7

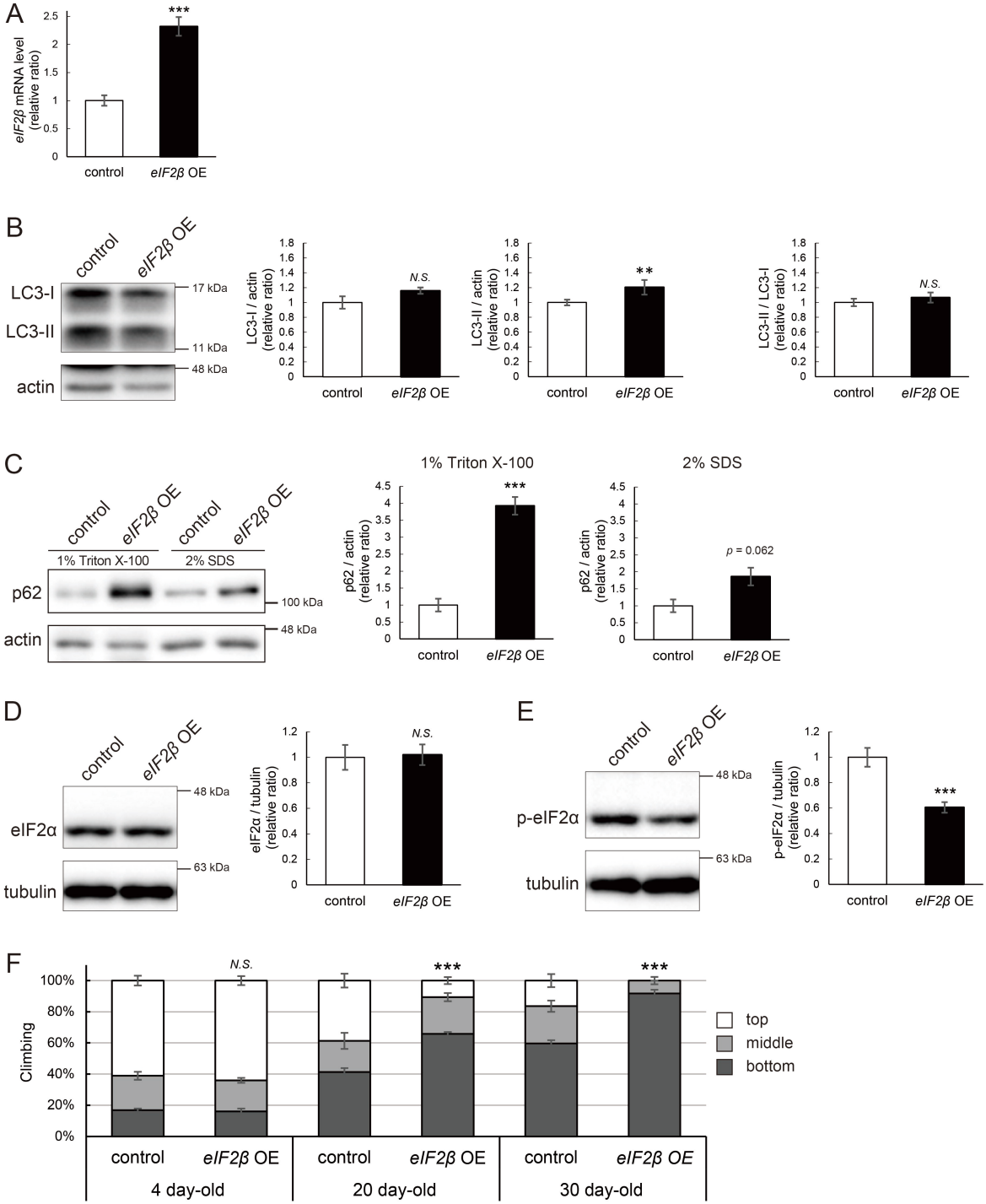

Shinno et. al., Figure 6

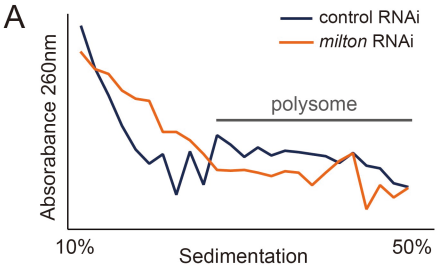

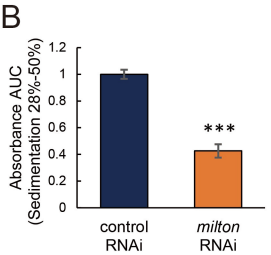

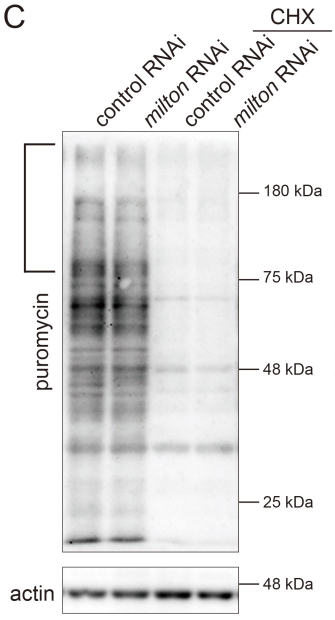

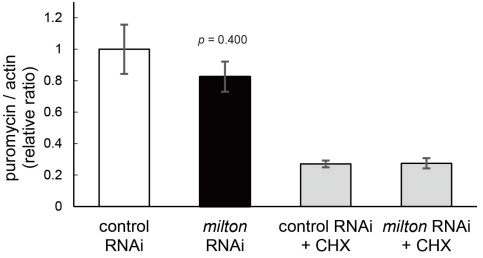

Shinno et. al., Figure 8

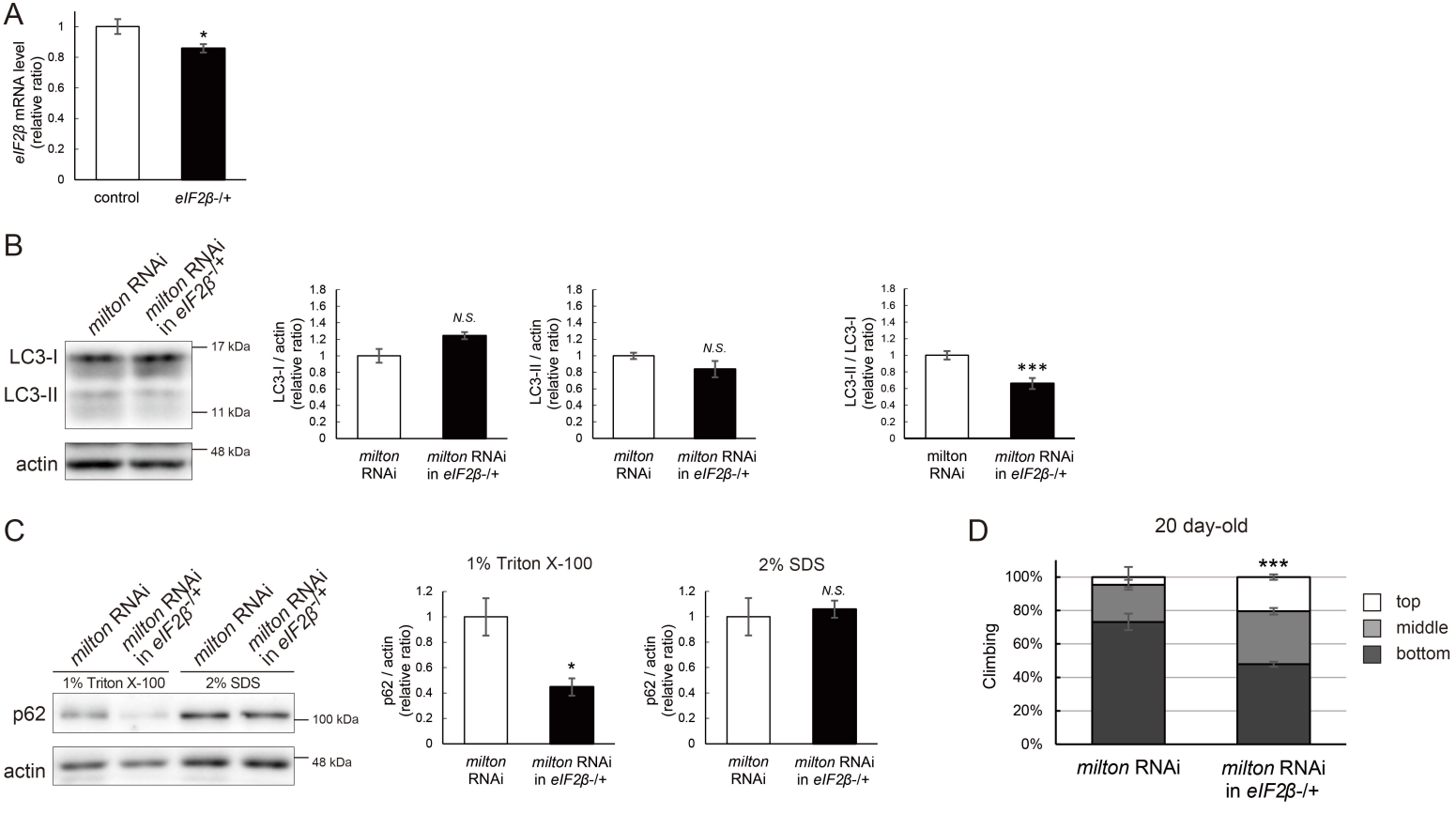

Shinno et. al., Figure 9

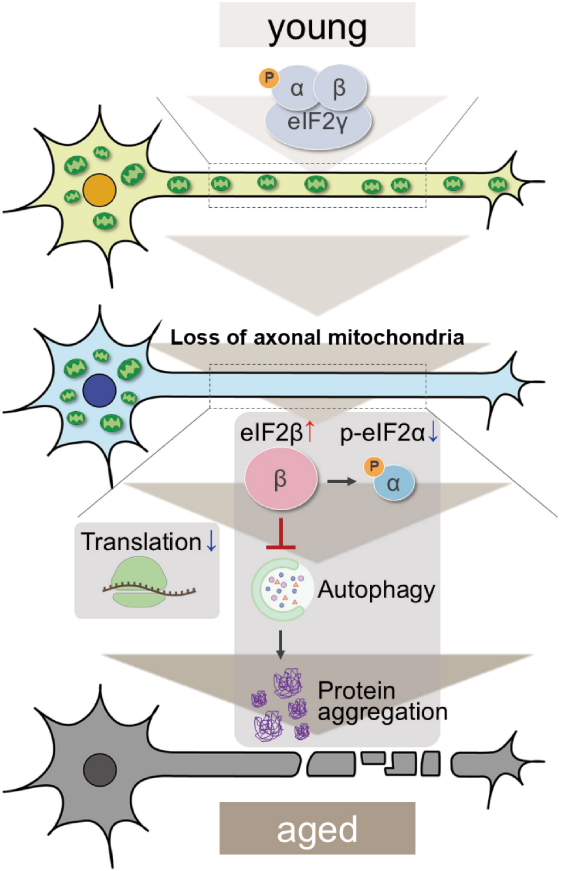

7 day-old			
Accession[a]	Name	Abundance Ratio: (7 days, milton KD) / (7 days, control)	Abundance Ratio P-Value: (7 days, milton KD) / (7 days, control)
Q9V751	Attacin-B	100	1E-17
Q04448	Bifunctional methylenetetrahydrofolate dehydrogenase/cyclohydrolase, mitochondrial	100	1E-17
P22700	Calcium-transporting ATPase sarcoplasmic/endoplasmic reticulum type	100	1E-17
Q9V558	Cytochrome P450 4p1	100	1E-17
P10552	FMRFamide-related peptides	100	1E-17
P05661-19	Isoform F of Myosin heavy chain, muscle	100	1E-17
Q9VE01	Probable cytochrome P450 12a5, mitochondrial	100	1E-17
Q7KIN0	Toll-like receptor 7	100	1E-17
Q8MKN0	Ubiquinone biosynthesis protein COQ9, mitochondrial	100	1E-17
Q9VJG0	Xaa-Pro aminopeptidase ApepP	100	1E-17
Q9V8F5	Bomanin Bicipital 1	4.908	1E-17
P07701	Salivary glue protein Sgs-5	2.843	1.99252E-09
Q76902	Pleckstrin homology domain-containing family F member 1 homolog	2.836	2.22045E-16
P81641	Alpha-amylase B	2.684	7.44847E-09
P19351-4	Isoform 4 of Troponin T, skeletal muscle	2.66	6.65563E-11
Q9VTJ8	Mitochondrial import inner membrane translocase subunit TIM14	2.61	3.54205E-07
P41375	Eukaryotic translation initiation factor 2 subunit 2	2.465	3.38486E-09
Q9VYB0	Selenoprotein BthD	2.462	2.25579E-08
B7Z0W9	Proton channel OtopLc	2.382	1.71741E-06
Q9VLR5	RNA polymerase II transcriptional coactivator	2.245	6.70245E-09
Q8IN44	Protein Turandot A	2.127	8.38662E-13
P27779	Pupal cuticle protein Edg-78E	2.113	1.00215E-08
Q9W1X8	Probable GDP-L-fucose synthase	0.496	2.12601E-08
P55035	26S proteasome non-ATPase regulatory subunit 4	0.487	5.50158E-11
Q9VHN6	39S ribosomal protein L19, mitochondrial	0.487	0.000551337
Q9VPD2	Cytosolic Fe-S cluster assembly factor NUBP2 homolog	0.46	6.34514E-05
Q9VHD3	Probable maleylacetoacetate isomerase 1	0.432	4.50956E-06
Q94529	Probable pseudouridine-5'-phosphatase	0.416	1.08802E-14
Q27606	Cytochrome P450 4e2	0.398	4.13128E-10
Q24388	Larval serum protein 2	0.378	1.33227E-14
Q9VKH6	Lysosomal thioesterase PPT2 homolog	0.369	2.05225E-06
Q24114	Division abnormally delayed protein	0.307	2.24406E-09
Q95NH6	Attacin-C	0.01	1E-17
P29993	Inositol 1,4,5-trisphosphate receptor	0.01	1E-17
Q94526	Open rectifier potassium channel protein 1	0.01	1E-17
Q9Y115	UNC93-like protein	0.01	1E-17

[a] UniProt accession number

21 day-old			
Accession[a]	Name	Abundance Ratio: (21 days, Milton KD) / (21 days, Control)	Abundance Ratio P-Value: (21 days, Milton KD) / (21 days, Control)
Q10714	Angiotensin-converting enzyme	100	1E-17
C0HKQ8	Cecropin-A2	100	1E-17
Q9V558	Cytochrome P450 4p1	100	1E-17
P51592	E3 ubiquitin-protein ligase hyd	100	1E-17
Q9VMJ7	Lysine-specific demethylase lid	100	1E-17
Q9VXP4	Platelet-activating factor acetylhydrolase IB subunit beta homolog	100	1E-17
Q9VY28	Probable 28S ribosomal protein S25, mitochondrial	100	1E-17
Q9W391	Probable phosphorylase b kinase regulatory subunit alpha	100	1E-17
Q9VUQ5	Protein argonaute-2	100	1E-17
P54359	Septin-2	100	1E-17
P24492	Diptericin A	15.716	1E-17
Q9VVY3	Glycogen-binding subunit 76A	8.986	1E-17
Q70PY2	Peptidoglycan-recognition protein SB1	6.669	1E-17
Q9W0M1	Centrosomal protein cep290	6.526	1E-17
P81641	Alpha-amylase B	5.722	1E-17
P45884	Attacin-A	4.997	1E-17
C0HL66	Histone H3.3A	4.778	1E-17
P26675	Protein son of sevenless	4.696	1E-17
P02515	Heat shock protein 22	4.69	1E-17
Q95NH6	Attacin-C	4.35	1E-17
P17971-1	Isoform A of Potassium voltage-gated channel protein Shal	4.195	1E-17
Q7K1U0	Activity-regulated cytoskeleton associated protein 1	3.271	1E-17
P14199	Protein ref(2)P	3.014	1E-17
Q9VU02	Probable small nuclear ribonucleoprotein Sm D1	2.43	4.91607E-13
Q9VD44	Poly(A) RNA polymerase gld-2 homolog A	2.268	2.6084E-11
Q9V8F5	Bomanin Bicipital 1	2.24	5.16671E-11
P22979	Heat shock protein 67B3	2.223	7.90048E-11
P27779	Pupal cuticle protein Edg-78E	2.192	1.65944E-10
Q9NBK5	Serine/threonine-protein kinase tricornered	2.059	4.15071E-09
Q8MLZ7	Chitinase-like protein Idgf3	2.055	4.61182E-09
Q9V751	Attacin-B	2.038	6.79416E-09
Q9V8M5	Probable 3-hydroxyisobutyrate dehydrogenase, mitochondrial	0.492	7.42952E-09
P84345	ATP synthase protein 8	0.421	1.809E-12
P33438	Glutactin	0.414	6.13731E-13
Q8IN44	Protein Turandot A	0.218	1E-17
Q8IN43	Protein Turandot C	0.195	1E-17
Q9VFI9	cGMP-specific 3',5'-cyclic phosphodiesterase	0.01	1E-17
Q94526	Open rectifier potassium channel protein 1	0.01	1E-17
Q9VHD3	Probable maleylacetoacetate isomerase 1	0.01	1E-17
Q9W0A0	Protein draper	0.01	1E-17
A1Z7T0	Serine/threonine-protein kinase N	0.01	1E-17

7 day-old					
Rank	Name	Score	Score (p) [a]	Score (v) [b]	Score (c) [c]
1	Autophagy-related protein signaling pathway	50.394	6.76E-16	0.159	0.11
2	Calcium signaling pathway	47.583	4.75E-15	0.146	0.117
3	Transcriptional regulation by SMAD	44.012	5.64E-14	0.146	0.095
4	GABA signaling pathway	40.706	5.58E-13	0.122	0.123
5	estrogen signaling pathway	37.507	5.12E-12	0.11	0.13
6	Sirtuin signaling pathway	36.87	7.96E-12	0.122	0.095
7	Transcriptional regulation by AP-1	34.874	3.18E-11	0.11	0.107
8	Arrestin signaling pathway	32.84	1.30E-10	0.11	0.092
9	G protein (Gq/11) signaling pathway	30.889	5.03E-10	0.085	0.149
10	Kainate receptor signaling pathway	30.049	9.00E-10	0.073	0.214
11	Transcriptional regulation by C/EBP	29.5	1.32E-09	0.098	0.093
12	Calpain signaling pathway	28.597	2.46E-09	0.11	0.066
13	Phospholipase D signaling pathway	28.344	2.94E-09	0.098	0.084
14	HSP90 signaling pathway	27.188	6.54E-09	0.085	0.104
14	CYP family	27.188	6.54E-09	0.085	0.104
16	Kir3 channel signaling pathway	26.495	1.06E-08	0.061	0.25
17	Estrogen biosynthesis	26.107	1.38E-08	0.061	0.238
18	CaSR signaling pathway	25.39	2.27E-08	0.061	0.217
19	PI3K signaling pathway	24.927	3.14E-08	0.073	0.122
20	PAF receptor signaling pathway	24.555	4.06E-08	0.049	0.4
21	Transcriptional regulation by PPARa	24.398	4.52E-08	0.073	0.115
21	BTK signaling pathway	24.398	4.52E-08	0.073	0.115
23	Transcriptional regulation by STAT	24.076	5.66E-08	0.085	0.077
24	G protein (Gi/o) signaling pathway	24.063	5.71E-08	0.073	0.111
25	PARP signaling pathway	23.742	7.13E-08	0.073	0.107
25	mGluR signaling pathway	23.742	7.13E-08	0.073	0.107
27	Free fatty acid signaling pathway	23.433	8.83E-08	0.073	0.103
28	Kir channel signaling pathway	23.338	9.43E-08	0.061	0.167
29	Oxytocin signaling pathway	23.327	9.51E-08	0.049	0.333
30	Transcriptional regulation by MEF2	22.99	1.20E-07	0.073	0.098
31	S100 family signaling pathway	22.434	1.77E-07	0.073	0.092
32	Transcriptional regulation by FOXO	22.301	1.94E-07	0.073	0.091
33	P2Y signaling pathway	22.172	2.12E-07	0.061	0.143
34	Transcriptional regulation by SRF	21.174	4.23E-07	0.061	0.125
34	ATF4/ATF6/IRE1 signaling pathway	21.174	4.23E-07	0.061	0.125
36	Chemerin signaling pathway	21.082	4.50E-07	0.049	0.235
36	Vasopressin signaling pathway	21.082	4.50E-07	0.049	0.235
38	Serotonin signaling pathway	20.854	5.28E-07	0.073	0.077
39	Transcriptional regulation by HIF	20.834	5.35E-07	0.098	0.043
40	Leukotriene receptorsignaling pathway	20.724	5.78E-07	0.049	0.222
40	CART signaling pathway	20.724	5.78E-07	0.049	0.222
42	MAPK signaling pathway	20.693	5.90E-07	0.085	0.055
43	Transcriptional regulation by RB/E2F	20.543	6.55E-07	0.098	0.042
44	NAD metabolism	20.468	6.89E-07	0.061	0.114
45	ERK signaling pathway	20.425	7.11E-07	0.073	0.073
46	Adenylyl Cyclase signaling pathway	20.303	7.73E-07	0.061	0.111
47	Bile acid signaling pathway	20.141	8.65E-07	0.061	0.109

[a] Score(p) indicates p-value of the pathway.
[b] Score(v) indicates the ratio of "Count" to total molecules associated with the loaded list.
[c] Score(c) indicates the ratio of "Count" to total molecules contained in the pathway.

21 day-old					
Rank	Name	Score	Score (p) [a]	Score (v) [b]	Score (c) [c]
1	Histone demethylation	84.198	4.51E-26	0.102	0.425
2	CDK inhibitor signaling pathway	56.497	9.83E-18	0.078	0.295
3	Transcriptional regulation by RB/E2F	46.598	9.39E-15	0.108	0.095
4	Mst(Hippo) signaling pathway)	46.343	1.12E-14	0.09	0.133
5	Transcriptional regulation by androgen receptor	46.078	1.35E-14	0.078	0.178
6	p160 SRC signaling pathway	45.809	1.62E-14	0.078	0.176
7	Transcriptional regulation by SMAD	43.961	5.84E-14	0.09	0.119
8	Autophagy-related protein signaling pathway	41.063	4.35E-13	0.084	0.119
9	Transcriptional regulation by HIF	39.527	1.26E-12	0.096	0.086
10	Nucleophosmin signaling pathway	38.417	2.72E-12	0.054	0.273
11	HSP90 signaling pathway	37.887	3.93E-12	0.066	0.164
12	PAF metabolism	37.562	4.93E-12	0.042	0.5
13	Transcriptional regulation by STAT	37.276	6.01E-12	0.072	0.132
14	Bcl-2 family signaling pathway	36.157	1.31E-11	0.072	0.124
15	Sirtuin signaling pathway	34.782	3.39E-11	0.072	0.114
16	Transcriptional regulation by C/EBP	33.819	6.60E-11	0.066	0.128
17	PIN1 signaling pathway	33.172	1.03E-10	0.06	0.149
18	RSK signaling pathway	30.566	6.29E-10	0.06	0.125
19	Transcriptional regulation by High mobility group protein	29.873	1.02E-09	0.054	0.148
20	BET family signaling pathway	29.656	1.18E-09	0.054	0.145
21	Transcriptional regulation by Myc	28.838	2.08E-09	0.066	0.093
22	Transcriptional regulation by FOXO	28.827	2.10E-09	0.054	0.136
23	PSD-95 family signaling pathway	26.154	1.34E-08	0.048	0.14
24	AKT signaling pathway	25.169	2.65E-08	0.048	0.129
25	Arginine methylation	24.799	3.43E-08	0.048	0.125
26	gp130 signaling pathway	24.25	5.01E-08	0.054	0.096
27	Transcriptional regulation by CREB	23.858	6.58E-08	0.066	0.067
28	Gene regulation by microRNAs (metastasis)	23.852	6.60E-08	0.054	0.093
29	HDAC signaling pathway	23.536	8.22E-08	0.036	0.207
30	Calpain signaling pathway	23.092	1.12E-07	0.06	0.074
31	Transcriptional regulation by IRF	22.738	1.43E-07	0.054	0.085
32	2-Oxoglutarate signaling pathway	22.673	1.50E-07	0.048	0.104
32	14-3-3 signaling pathway	22.673	1.50E-07	0.048	0.104
34	Transcriptional regulation by POU domain factor	22.601	1.57E-07	0.06	0.071
35	Transcriptional regulation by BLIMP-1	22.474	1.72E-07	0.042	0.132
36	Gene regulation by microRNAs (metabolism)	22.39	1.82E-07	0.054	0.083
37	Fatty acid beta oxidation	22.096	2.23E-07	0.042	0.127
38	Transcriptional regulation by RXR	22.08	2.26E-07	0.036	0.176
39	ERK signaling pathway	21.96	2.45E-07	0.048	0.098
40	PARP signaling pathway	21.913	2.53E-07	0.042	0.125
41	Transcriptional regulation by VDR	21.618	3.11E-07	0.054	0.078
42	Transcriptional regulation by p53	21.168	4.24E-07	0.072	0.05
43	Acetylcholine metabolism	21.152	4.29E-07	0.024	0.444
44	Gene regulation by microRNAs (embryonic stem cells)	21.08	4.51E-07	0.036	0.158
45	mTOR signaling pathway	21.048	4.61E-07	0.042	0.115
46	Gene regulation by microRNAs (cancer)	21.04	4.64E-07	0.048	0.09
47	Transcriptional regulation by Ets-1/2	20.724	5.77E-07	0.042	0.111
48	MAPK signaling pathway	20.411	7.18E-07	0.054	0.07
49	Gene regulation by microRNAs (cell cycle)	20.404	7.21E-07	0.036	0.146
50	Transcriptional regulation by p73	20.259	7.97E-07	0.042	0.106